Hindawi
Mathematical Problems in Engineering
Volume 2020, Article ID 6531984, 24 pages
https://doi.org/10.1155/2020/6531984

Research Article

Trajectory Planning and Tracking for Carrier Aircraft-Tractor System Based on Autonomous and Cooperative Movement

Minghui Yu,[1] Xue Gong,[1] Guowei Fan,[2] and Yu Zhang[2]

[1]*School of Artificial Intelligence and Automation, Huazhong University of Science and Technology, Wuhan 430074, China*
[2]*China Ship Development and Design Center, Wuhan 430064, China*

Correspondence should be addressed to Xue Gong; gongxue@hust.edu.cn

Received 5 March 2020; Accepted 29 April 2020; Published 13 June 2020

Guest Editor: Xiao Ling Wang

The solution of how to plan out the cooperative moving trajectory autonomously and control the motion of carrier-based aircraft timely and accurately is the key to helping improve the overall deck operation efficiency. The main problem discussed in this article is coordinated trajectory planning strategy for multicarrier aircraft and cooperative control between tractor and carrier aircraft. First, the kinematic model and three-degree-of-freedom dynamics model of the towbarless traction system are established. Then, a coevolution mechanism for aircraft systems is proposed to ensure coordinated trajectory planning among multiple aircraft and a trajectory adapted to the tractor-aircraft system is generated based on the hybrid RRT* algorithm. Next, a double-layer closed-loop controller is designed for the trajectory tracking of the tractor-aircraft system on the deck under the constraints of incomplete constraints and various physical conditions. It includes an outer model predictive controller which effectively controls the cooperative motion between the carrier aircraft and tractor and an inner torque control strategy based on adaptive fuzzy PID control which strictly ensures the stability of the system. Simulation results demonstrate that the controller is more rapid, more accurate, and more robust in tracking line trajectory with initial deviation, sine curve with large curvature, and complex trajectories on decks compared with backstepping control and LQR algorithm.

1. Introduction

Aircraft carrier is one of the extra-large maritime combat platforms. The number and the launch-recovery efficiency of carrier-based aircraft is quite important for the platform's combat effectiveness. The efficiency and safety of transfer operations in hangar and flight deck directly affect the launching efficiency of carrier-based aircraft. At present, the dispatching operation mainly adopts the coordinated control method of the tractor and guide. However, with the rapid development of the intelligent industry, automatic tractors will become the trend of ground movement of carrier-based aircraft, which will place further demands on the speed and safety of carrier-based aircraft's movement. Path planning is one of the most important links in transportation operations and many scholars have done research [1, 2]. To the best of our knowledge, there is little research to deal with the problem of cooperative trajectory generation of multiple aircraft traction systems. At the same time, there are numerous shortages and restrictions in practice [3–8]. Due to the complicated movement process of the tractor-aircraft system, the planned trajectory is generally under ideal conditions, which means it is difficult to consider the error factors such as the initial deviation [9–11]. Therefore, the quality of trajectory tracking is a key factor in judging the overall control system.

The trajectory tracking problem of carrier-based aircraft traction system is defined as follows: the system starts from an initial position on the hangar or flight deck, moves along a desired time-related trajectory under the controller, and finally reaches the specified position steadily. Moreover, the core of the research is to design the controller to make the tracking accuracy higher. Trajectory tracking problem of tractor-aircraft system on deck has not been explored to a large extent. If the factors such as the mass of the aircraft and the constraints of trajectory planning are ignored, it can be

regarded as a drag-pull system to a certain degree. According to the structural characteristics of the traction system, the aircraft can be regarded as a trailer. The main goal is to track the trajectory of the aircraft, so that the aircraft can reach the predetermined position according to the ideal trajectory as much as possible. Many studies about the trajectory tracking of the tractor system have been carried out and many representative methods have been proposed during the past decades.

For the preliminary research of trajectory tracking problems, traditional control methods are mainly used, such as PID control or sliding mode control (SMC) [12]. Due to the complex kinematics and dynamics of the tractor system, the performance of the trajectory tracking system designed by the classic control method is quite limited, which makes the controller must be adjusted in an adaptive manner [13]. It is convenient to use the PID controller for Simple Input Simple Output (SISO) systems, while tractor-trailer systems have multiple inputs and outputs. Traditionally, decentralized control is performed by designing a controller for each SISO subsystem, but it is difficult to consider the interaction between each system [14]. Therefore, control method of dynamic state feedback has been proposed. For the towed wheeled mobile robot (TTWR), Khalaji and Moosavian proposed a robust adaptive feedback linearized dynamic controller (RAFLDC) and verified the stability of the control algorithm using the Lyapunov method [15]. Huofeng et al. designed a linear dynamic feedback controller based on the internal model principle, which can ensure the boundedness of the tracking error [16]. A controller that combines kinematics and dynamics has been created by Lashkari [17]. The speed input of the system is determined by the kinematic controller, and then the required torque of the trailer is calculated to achieve the given speed input. This method guarantees the stability of the controller and can adjust the parameters according to the number of trailers. In addition, linear quadratic regulator- (LQR-) based controllers are widely applied in the field of trajectory tracking. A linear secondary regulator was proposed in [18] to control the position of the trailer. However, it has been pointed out that feedforward control is needed to compensate for the curve with large curvature.

Model predictive control (MPC) has developed rapidly in recent decades, but too little work has been devoted to the trajectory tracking of carrier-based aircraft. In the trajectory tracking of mobile robots, the nonlinear model is usually linearized first and then transformed into a linear time-invariant system for control. Bin et al. developed a control framework based on the MPC method and used hybrid logic dynamics (MLD) to model the axleless tractor-trailer system. Then, a hybrid integer quadratic programming method is used to design an optimal reversing controller [19]. Yue et al. designed a dynamic controller based on MPC and SMC. The latter drives the vehicle's speed to track the expected speed generated by the former, which guarantees the progressive convergence of the inner loop from the perspective of stability [20]. Kayacan et al. created a control method based on linear model predictive controller and combined it with feedforward control and robust control [21]. At the same time, some scholars have applied nonlinear model predictive control to the trajectory tracking of tractor-trailer systems. In [22], Backman et al. studied the NMPC implementation of the tractor-trailer system, which can control them to track straight lines and curves. Reference [23] Mentioned a nonlinear rolling time-domain estimator and a nonlinear model predictive controller based on an adaptive model and gave relatively successful experimental results. Unfortunately, NMPC requires a very large amount of calculations [24]. Although its tracking accuracy is good, it is still difficult to achieve online real-time controlling.

There are three main ways of carrier-based aircraft movement on aircraft carriers: aircraft taxi motion, towbarless tractor traction motion, and towbar tractor traction motion. Shipboard aircraft do not have the conditions for taxiing on aircraft carrier decks with relatively narrow spaces, compact deployments, and inaccessibility. The towbarless tractor uses its own clamping and lifting device to directly act on the aircraft's front landing gear. This method does not require a towbar to connect to the aircraft, which is more flexible than a towbar tractor [25]. In view of the above problems, this paper focuses on the trajectory tracking model of the towbarless traction system.

This article is highly motivated by the strong demand in the military and other related fields. We expect to employ advanced control technology to help the aircraft reach the designated position quickly and accurately, so as to increase the flight sorties rate. The summary of our contributions is listed as follows.

(1) We describe a novel application scenario (i.e., towbarless tractor-aircraft trajectory tracking) for model predictive control (MPC). A full-state controller is designed through MPC to drive all state variables to converge to the desired trajectory.

(2) We generate trajectories suitable for the carrier aircraft on the deck using the hybrid RRT* algorithm based on the collaborative strategy and convex the obstacles on deck and define a distance function that is particularly suitable for carrier aircraft. Taking into account the driving characteristics of carrier-based aircraft, the RRT node is expanded using the Reeds-Shepp route, which is different from other path planning algorithms.

(3) In order to improve the dynamic stability of the system, we propose a self-adaptive fuzzy PID controller to control the system's centroid yaw and yaw rate by adding yaw moment.

(4) We conduct many sets of simulation experiments to verify the effectiveness and advantages of the method for this scenario.

In the remainder of this paper, the description of the towbarless tractor-aircraft system is introduced in Section 2, the trajectory generation and trajectory tracking controller are proposed in Section 3 and Section 4, respectively. Section 5 shows experimental results of different trajectory. The conclusion of this paper is presented in Section 6.

2. Towbarless Tractor-Aircraft System

Consider a towbarless traction system with carrier aircraft, as sketched in Figure 1. In the inertial coordinate system OXY, $P_1(x_1, y_1)$ and $P_2(x_2, y_2)$ are the position coordinates of the tractor and the aircraft; θ_1 and θ_2 are the direction angles of the tractor and the carrier. δ is the steering angle of the front wheels and v is the axial speed of the rear axle of the tractor.v_i and ω_i are the lateral speed and yaw rate of the tractor and the aircraft, respectively. m_i and I_i are the mass and moment of inertia of the tractor and the aircraft, respectively. F_{x_i} and F_{y_i} are the longitudinal and lateral forces on the tires of the tractor and the aircraft, and T is the steering torque, where $i = 1, 2$.

For its motion on the deck, the following assumptions are made:

(a) Assuming a pure rolling motion, both the tractor and the aircraft are rigid bodies

(b) Both the tractor and the carrier aircraft are symmetrical along the longitudinal axis

(c) The aircraft's front landing gear is directly articulated at the midpoint of the two rear wheels of the tractor

(d) Regardless of the effects of air resistance and friction, only the lateral movement of the tractor along the y-axis and the yaw movement around the center of mass are considered

2.1. Kinematic Model. When the speed of the traction system is small, the kinematics model can better describe the motion of the system [26]. According to the incomplete constraints of the towbarless tractor system, the kinematic relationship of the system can be simplified. The kinematic equation of the carrier-based traction system is described as follows:

$$\begin{cases} \dot{x}_1 = v\cos\theta_1, \\ \dot{y}_1 = v\sin\theta_1, \\ \dot{\theta}_1 = \dfrac{v\tan\delta}{L_1}, \\ \dot{x}_2 = v\left[\cos(\theta_1 - \theta_2)\cos\theta_2\right], \\ \dot{y}_2 = v\left[\cos(\theta_1 - \theta_2)\sin\theta_2\right], \\ \dot{\theta}_2 = \dfrac{v\sin(\theta_1 - \theta_2)}{L_2}. \end{cases} \tag{1}$$

According to the geometric relationship between the two adjacent car bodies in the trailer system, the complete system constraints are obtained:

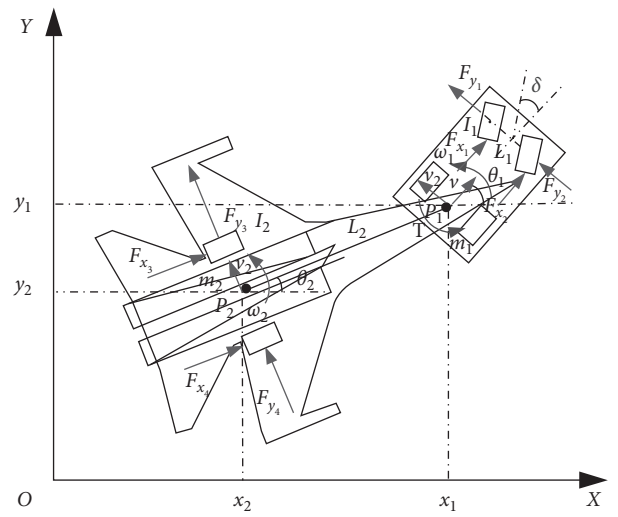

Figure 1: Towbarless traction system with carrier aircraft.

$$\begin{bmatrix} x_1 \\ y_1 \end{bmatrix} = \begin{bmatrix} x_2 \\ y_2 \end{bmatrix} + L_2 \begin{bmatrix} \cos\theta_2 \\ \sin\theta_2 \end{bmatrix}. \tag{2}$$

The main task of trajectory tracking is to track the movement trajectory of the carrier-based aircraft, so that the carrier-based aircraft can reach the target position quickly and accurately. Therefore, the configuration of the whole system is completely given by $(\theta_1, x_2, y_2, \theta_2)$. The state variable is $\xi = [\theta_1, x_2, y_2, \theta_2]^T \in \Omega$, the output variable is $Y = [\theta_1, x_2, y_2, \theta_2]^T$, and the control variable is $U = [v, \delta]^T \in \psi$. The system can be expressed as the following state space expression:

$$\dot{\xi}_0 = f(\xi_0, u_0). \tag{3}$$

Since the linearized system is simple to control and easy to solve, we linearize the above model.

$$\dot{\xi} = f(\xi_0, u_0) + A(t)(\xi - \xi_0) + B(t)(u - u_0). \tag{4}$$

Subtracting (3) and (4), we get

$$\dot{\widetilde{\xi}} = A(t)\widetilde{\xi} + B(t)\widetilde{u}, \tag{5}$$

where $\widetilde{\xi} = \xi - \xi_0$, $\widetilde{u} = u - u_0$, $A(t) = (\partial f/\partial\xi)|_{\xi_0, u_0}$, and $B(t) = (\partial f/\partial u)|_{\xi_0, u_0}$.

This state space expression is continuous. The linear parameter-varying (LVP) model after discretization is described as

$$\begin{cases} \widetilde{\xi}(k+1) = A_{k,t}\widetilde{\xi}(k) + B_{k,t}\widetilde{u}(k), \\ \eta(k) = C_{k,t}\widetilde{\xi}(k), \end{cases} \tag{6}$$

where

$$A_{k,t} = \begin{bmatrix} 0 & 0 & 0 & 0 \\ -\sin(\theta_1-\theta_2)\cos\theta_2 vt & 0 & 0 & [-\sin(\theta_1-\theta_2)\cos\theta_2 - \cos(\theta_1-\theta_2)\sin\theta_2]vt \\ -\sin(\theta_1-\theta_2)\sin\theta_2 vt & 0 & 0 & [-\sin(\theta_1-\theta_2)\sin\theta_2 - \cos(\theta_1-\theta_2)\cos\theta_2]vt \\ \dfrac{vt\cos(\theta_1-\theta_2)}{L_2} & 0 & 0 & -\dfrac{\cos(\theta_1-\theta_2)vt}{L_2} \end{bmatrix},$$

$$B_{k,t} = \begin{bmatrix} \dfrac{t\tan\delta}{L_1} & \dfrac{vt}{L_1\cos^2\delta} \\ \cos(\theta_1-\theta_2)\cos\theta_2 t & 0 \\ \cos(\theta_1-\theta_2)\sin\theta_2 t & 0 \\ \dfrac{t}{L_2}\sin(\theta_1-\theta_2) & 0 \end{bmatrix}. \tag{7}$$

Let $\widehat{\xi}(k\,|\,t) = \begin{bmatrix} \xi(k\,|\,t) \\ u(k-1\,|\,t) \end{bmatrix}$; then get the new state equation as

$$\begin{cases} \widehat{\xi}(k+1) = A_t\widehat{\xi}(k\,|\,t) + B_t\Delta u(k), \\ \eta(k) = C_t\widehat{\xi}(k\,|\,t), \end{cases} \tag{8}$$

where $A_t = \begin{bmatrix} A_{k,t} & B_{k,t} \\ 0_{2\times4} & I \end{bmatrix}$, $B_t = \begin{bmatrix} B_{k,t} \\ I \end{bmatrix}$, and $C_t = \begin{bmatrix} C_{k,t} & 0_{4\times2} \end{bmatrix}$.

2.2. Dynamics Model. When the traction system's speed is large, the dynamic stability of the system needs to be considered. The three-degree-of-freedom dynamics equation of tractor-aircraft system is established based on Newtonian mechanics [27]:

$$\begin{cases} m_1a_{y_1} + m_2a_{y_2} - \left(F_{y_1}+F_{y_2}\right) - \left(F_{y_2}+F_{y_4}\right) = 0, \\ \left(I_1 + m_1L_1^2\right)\dot{\omega}_1 - \left(F_{y_1}+F_{y_2}\right)L_1 - F_{x_1}b + F_{x_2}b - T = 0, \\ \left(I_2 + m_2L_2^2\right)\dot{\omega}_2 + \left(F_{y_3}+F_{y_4}\right)L_2 - F_{x_3}c + F_{x_4}c + T = 0. \end{cases} \tag{9}$$

Among them, b and c are one-half of the wheel gap between the tractor and the aircraft, respectively, a_{y_1}, a_{y_2} are the centroid accelerations of the tractor and the aircraft, and

$$\begin{cases} a_{y_1} = \dot{v}_1 + v\omega_1, \\ a_{y_2} = \dot{v}_1 - L_2\dot{\omega}_1 + L_2\ddot{\psi} + v\omega_1, \psi = \theta_1 - \theta_2, \dot{\theta}_1 = \omega_1, \dot{\theta}_2 = \omega_2. \end{cases} \tag{10}$$

When the system travels along a curve with a large curvature, the steering system is equivalent to a torsion spring acting on the hinge point, and the spring stiffness is represented by K_ψ. Then, the steering torque T, the tire yaw angle $\beta_i\,(i = 1, 2, 3, 4)$, the tractor yaw angle β_{tractor}, and the lateral force $F_{y_i}\,(i = 1, 2, 3, 4)$ are as follows:

$$T = -K_\psi\psi, \tag{11}$$

$$\beta_1 = \beta_2 = \frac{v_1 + L_1\omega_1}{v}, \tag{12}$$

$$\beta_3 = \beta_4 = \frac{v_1 - L_2\omega_1 + L_2\dot{\psi}}{v}, \tag{13}$$

$$\beta_{\text{tractor}} = \frac{v_1}{v}, \tag{14}$$

$$F_{y_1} = F_{y_2} = k_1\beta_1, \tag{15}$$

$$F_{y_3} = F_{y_4} = k_2\beta_3, \tag{16}$$

where k_1 and k_2 are the tire cornering stiffness. According to equations (9)~(16), the state equations in matrix form can be obtained:

$$M\dot{X} + JX = H, \tag{17}$$

where M is the system inertia matrix, J is the Jacobian state matrix, and the state variable $X = [v_1\ \omega_1\ \omega_2\ \psi]^T$.

In order to study the stability of the system, this paper uses an additional torque to drive the tractor-aircraft system to run stably. Applying torque $\pm F_x$ to the left and right front wheels of the tractor is equivalent to applying yaw moment $M\prime$ to the entire body. By integrating equations (14) and (17), the dynamics model of the entire system is obtained as follows:

$$\dot{X}' = AX' + B\dot{\psi} + C\psi + LM'. \tag{18}$$

Among them,

$$A = \begin{bmatrix} a_{11} & a_{12} \\ a_{21} & a_{22} \end{bmatrix},$$

$$B = \begin{bmatrix} b_1 \\ 0 \end{bmatrix},$$

$$C = \begin{bmatrix} c_1 \\ c_2 \end{bmatrix},$$

$$L = \begin{bmatrix} 0 \\ h_2 \end{bmatrix},$$

$$X' = \begin{bmatrix} \beta_{\text{tractor}} \\ \omega_1 \end{bmatrix},$$

$$h_2 = \frac{1}{I_1},$$

$$a_{11} = \frac{2(k_1 + k_2)}{(m_1 + m_2)v} - \frac{2m_2 k_2 L_2^2}{(I_2 + m_2 L_2^2)(m_1 + m_2)v},$$

$$a_{12} = \frac{2k_2 m_2 L_2^3}{(I_2 + m_2 L_2^2)(m_1 + m_2)v^2} + \frac{2k_1 L_1 - 2k_2 L_2}{(m_1 + m_2)v^2} - 1,$$

$$a_{21} = \frac{2k_1 L_1}{I_1},$$

$$a_{22} = \frac{2k_1 L_1^2}{I_1 v},$$

$$c_2 = \frac{K_\psi}{I_1},$$

$$b_1 = \frac{2k_2 L_2}{(m_1 + m_2)v^2} - \frac{2k_2 m_2 L_2^2}{(I_2 + m_2 L_2^2)(m_1 + m_2)v^2},$$

$$c_1 = \frac{m_2 K_\psi L_2 - 2m_2 k_2 L_2^2}{(I_2 + m_2 L_2^2)(m_1 + m_2)v} + \frac{2k_2}{(m_1 + m_2)v}. \tag{19}$$

This dynamics model considers the differential term of the articulation angle and controls the system's centroid yaw and yaw rate through additional torque.

3. Path Planning and Trajectory Generation

3.1. Collaborative Strategy for Tractor-Aircraft System. When a carrier-based aircraft moves on the deck, the state of other carrier-based aircraft and environmental information will affect its movement trajectory, and the information collected from only one aircraft is quite limited. Therefore, the current operation trend is that the "Captain" in the system manages the transfer of all carrier aircraft and organizes the basic communication between the aircraft. Through the communication between different carrier aircrafts, the coordinated trajectory planning can be carried out for a dispatching task, so as to avoid all obstacles and seek the overall optimal route. In this mode, coordinate position, speed, steering angle, attitude, and other information of each other can be communicated. Each carrier aircraft has its own local trajectory planner and trajectory tracking controller. Figure 2 shows the coordination mechanism in the process of carrier aircraft dispatching. This mechanism not only considers the behavior of a single carrier aircraft but also considers the state of other carrier aircraft moving on the deck [28].

Through the above cooperation mechanism, we can complete trajectory generation and obstacle avoidance, and the overall controller design of a single aircraft is as follows.

According to the kinematics and dynamics model established in Section 2, we establish the control structure shown in Figure 3. First, the feasible path is generated by RRT*. Second, in order to meet the various constraints of the system, a model predictive controller is designed to track the trajectory, and GA is used to iteratively optimize the parameters of MPC. Next, considering the disturbance factors when the system turns, it may have different degrees of influence on the dynamic performance of the vehicle, so an adaptive fuzzy PID controller is designed to observe and improve the stability of the system. The meaning of the variables in the figure will be defined in the following paragraphs.

3.2. RRT Algorithm Based on Reeds-Shepp.* When the carrier-based aircraft is towed from the initial position to the target position on the deck, it is essential to achieve the optimal path while avoiding all obstacles. In order to track the mission route on the deck, this paper first uses RRT* algorithm to search the optimal path.

The RRT algorithm is a random algorithm that covers the search space by constructing tree nodes. This method can easily add obstacle constraints when expanding nodes. Using feature graphics to describe the obstacles on the deck, the folded and spread wings of the carrier-based aircraft can be simplified into two different shapes of convex edges, as shown in the Figure 4. When the carrier-based aircraft is regarded as an obstacle, the length of the vertical line between the center point of the traction system and the convex contour of the obstacle must exceed the safety distance between the two carrier-based aircraft.

Different from the ordinary RRT algorithm, the Reeds-Shepp path is used when expanding nodes. Reeds-Shepp path is a kind of shortest path composed of straightforward, backward, turn left, turn right, and other basic curves [29]. By limiting the curvature of the curve, it is ensured that the traction system has a sufficient turning radius and is more in line with the actual movement of the carrier-based aircraft.

The hybrid RRT* algorithm flow is shown in Figure 5. First, the starting node *q_start* is used as the root node to build the search tree *Tree*. The node *q_rand* is obtained by random sampling. After traversing the *Tree* to find the node *q_nearest* closest to *q_rand*, the Reeds-Shepp path between

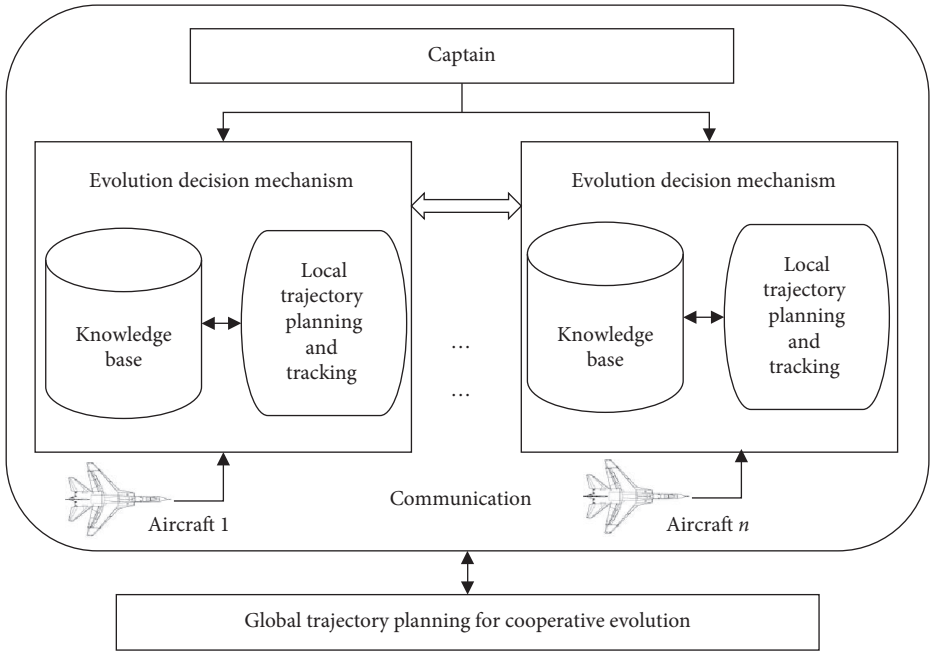

Figure 2: Mechanism of coevolution for aircraft systems.

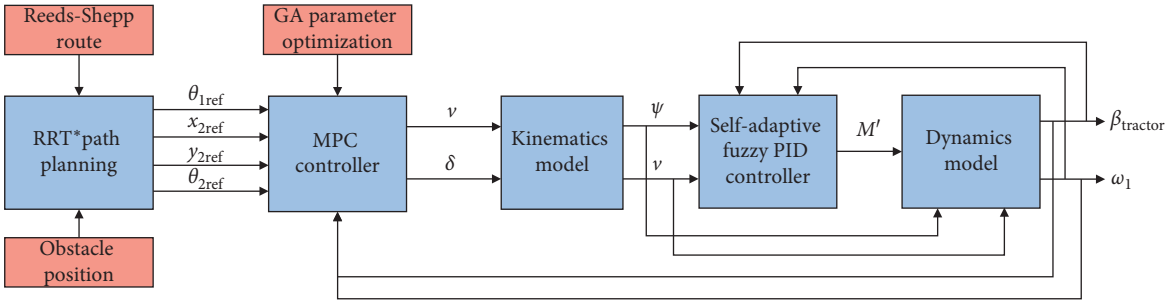

Figure 3: Block diagram of control structure.

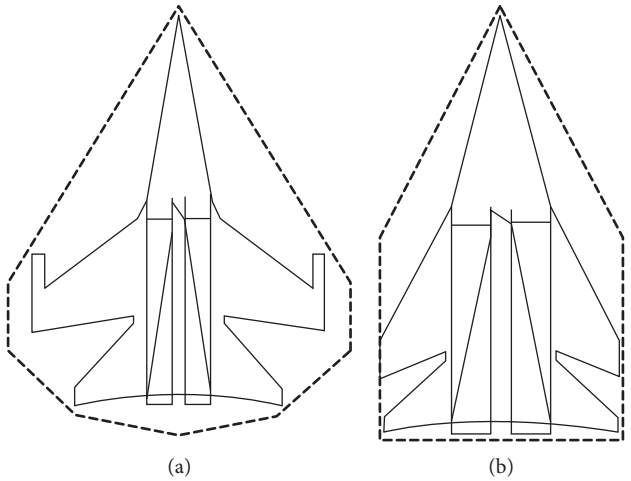

Figure 4: Convex outline of (a) spread and (b) folded wings.

```
Generate_Path(q_start, q_goal, max_iter, obstacle)
Tree ← q_start
for i = 1 to max_iter do
  q_rand ← Random_Node()
  q_nearest ← Nearest_Node(Tree, q_rand)
  q_new ← New_Node_ByRS(q_rand, q_nearest)
  if no_collision(q_new, obstacle)
    near_nodes ← Near_Nodes(q_new)
    q_new ← Select_Parent(near_nodes)
    if q_new
      Tree.add_node(q_new)
q_last ← Best_Goal_Node(Tree, q_goal)
if q_last return q_last
else return None
```

Figure 5: Hybrid RRT* algorithm pseudocode.

the two is generated and stored in the new node *q_new*. Collision detection is performed on the generated path. If it is within a safe distance, the parent node of *q_new* is searched again in the *Tree*. It is required that the path cost between this parent node and *q_new* be minimal and there is no collision. If *q_new* exists, it is added to the random expansion tree as a new leaf node. The above process is continuously iterated until the maximum number of generations is exceeded, and the search is ended. The target node *q_goal* is traced back to the starting node *q_start*, and the planned path is obtained.

In the above algorithm, to calculate the distance between two nodes, Euclidean distance can usually be used in systems with complete constraints. But, for the traction system in this article, more consideration should be given to its own motion characteristics. The direction angle is an important factor in determining whether the system needs to make a large turn. In order to obtain a more accurate distance measurement and reduce the amount of calculation, the approximate distance is employed in (20) [30]. Among them, R is the minimum turning radius, and O_1 and O_2 are the centers of the circles on both sides with Q_0 as the center, as shown in Figure 6.

$$D(Q_0, Q_1) = \begin{cases} 2\pi R, & \text{if } \|O_1 - Q_1\| < R \text{ or } \|O_2 - Q_1\| < R, \\ \|Q_1 - Q_0\|, & \text{otherwise.} \end{cases} \tag{20}$$

The final distance can be expressed as

$$M(Q_0, Q_1) = \sqrt{D^2(Q_0, Q_1) + \alpha(\varphi_0 - \varphi_1)}, \tag{21}$$

where φ is the direction angle of the point and α is the weight of φ.

Premeditating the adverse effect of the turn on the movement, the weighted sum of the path length and the number of turns is applied as the calculation standard of the path cost. The weight of the number of turns can be expressed by β.

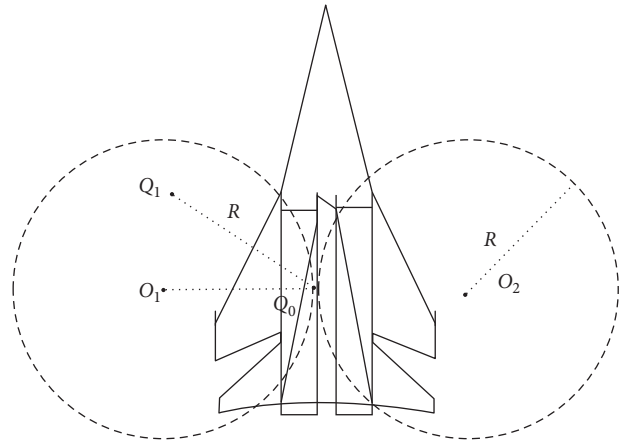

Figure 6: Circle with the minimum turning radius.

$$\text{cost} = \sum l + \beta \sum \text{turns}. \tag{22}$$

3.3. Reference Trajectory Generation. In the tracking problem, the generated path will be transformed into an allowable trajectory, that is, the solution of the differential equation of the traction system motion model [31]. The reference trajectory can be indicated as

$$\begin{aligned} x_{2r} &= x(t), \\ y_{2r} &= y(t). \end{aligned} \tag{23}$$

From the kinematics model of equation (1), we can get

$$v_r = \pm \sqrt{\left(\frac{dx_{1r}}{dt}\right)^2 + \left(\frac{dy_{1r}}{dt}\right)^2}, \tag{24}$$

where $x_{1r} = x_{2r} + l_2 \cos\theta_{2r}$, $y_1 = y_{2r} + l_{2r} \sin\theta_{2r}$.

Simultaneously,
$\theta_{2r} = \arctan(y'_{2r}/x'_{2r}) = (y''_{2r}x'_{2r} - y'_{2r}x''_{2r})/x'^2_{2r} + y'^2_{2r}$ and $\theta_{1r} = \theta_{2r} + \arctan(l_{2r}\theta'_{2r}/v_r)$. So far, the system's reference trajectory input $[\,\theta_{1\text{ref}} \;\; x_{2\text{ref}} \;\; y_{2\text{ref}} \;\; \theta_{2\text{ref}}\,]^T$ is obtained, and the reference trajectory and its derivatives are continuous and uniformly bounded [4].

4. Trajectory Tracking

Aiming at the various state constraints of the system, we use a model predictive controller to track any reference trajectory and then achieve control of the driving torque through adaptive control in dynamics.

4.1. Model Predictive Controller

4.1.1. Controller Design. According to the discrete linearized state equation in Section 2.1, the trajectory tracking control is performed using the model predictive control method. The design structure of the controller is shown in Figure 7.

Let N_p be the predicted time domain and N_c be the control time domain; the system output in the predicted time domain can be presented by the following formula:

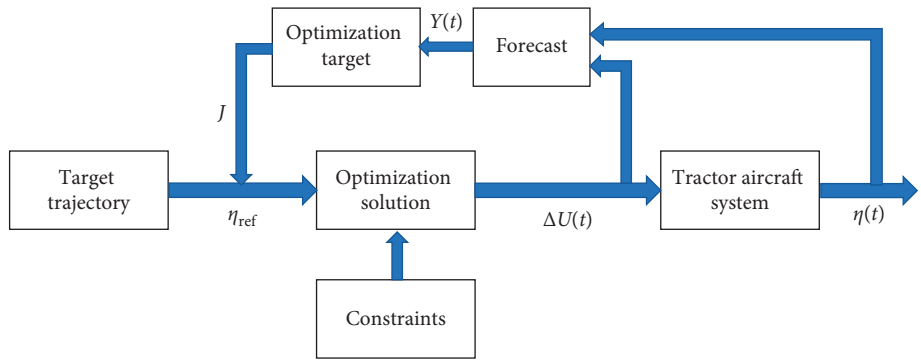

Figure 7: Structure of MPC controller.

$$Y(t) = \begin{bmatrix} \eta(t+1\,|\,t) \\ \eta(t+2\,|\,t) \\ \vdots \\ \eta\left(t+N_p\,|\,t\right) \end{bmatrix}. \tag{25}$$

The system input is defined as the amount of change in the input variable at each moment in the control time domain:

$$\Delta U(t) = \begin{bmatrix} \Delta u(t\,|\,t) \\ \Delta u(t+1\,|\,t) \\ \vdots \\ \Delta u\left(t+N_c\,|\,t\right) \end{bmatrix}. \tag{26}$$

Then, the prediction output in the system prediction time domain can be formulated by

$$Y(t) = \psi_t \xi(t\,|\,t) + \Lambda_t \Delta U(t), \tag{27}$$

where

$$\psi_t = \begin{bmatrix} C_t A_t \\ C_t A_t^2 \\ \vdots \\ C_t A_t^{N_p-1} \end{bmatrix},$$

$$\Lambda_t = \begin{bmatrix} C_t B_t & 0 & 0_{4\times2} & 0_{4\times2} \\ C_t A_t B_t & C_t B_t & 0_{4\times2} & 0_{4\times2} \\ \vdots & \vdots & \ddots & \vdots \\ C_t A_t^{N_c-1} B_t & C_t A_t^{N_c-2} B_t & \cdots & C_t B_t \\ C_t A_t^{N_c} B_t & C_t A_t^{N_c-1} B_t & \cdots & C_t A_t B_t \\ \vdots & & \ddots & \vdots \\ C_t A_t^{N_p-1} B & C_t A_t^{N_p-2} B & \cdots & C_t A_t^{N_p-N_c-1} B \end{bmatrix}. \tag{28}$$

The purpose of designing the controller is to enable the carrier-based aircraft to track the target trajectory quickly and with as little error as possible and make it possible for the change of the control amount to be smoother. The objective function J mainly considers the tracking performance of the controller.

$$J_1 = \sum_{i=1}^{N_p} \left\| \eta(t+i\,|\,t) - \eta_{\text{ref}}(t+i\,|\,t) \right\|_Q^2, \tag{29}$$

where Q is the output weighting matrix and $\eta_{\text{ref}} = [\,\theta_{1\text{ref}} \;\; x_{2\text{ref}} \;\; y_{2\text{ref}} \;\; \theta_{2\text{ref}}\,]^T$ is the reference trajectory. At the same time, the control variable is considered to make the control variable change to the minimum in the control time domain:

$$J_2 = \sum_{i=1}^{N_c-1} \left\| \Delta u(t+i\,|\,t) \right\|_R^2, \tag{30}$$

where R is the control weighting matrix. At the same time, a relaxation factor ε is added to ensure that the system that changes in real time has a feasible solution at every moment. The final objective function is:

$$\min J = J_1 + J_2 + \sigma\varepsilon^2. \tag{31}$$

In the actual control system, constraints such as control variable constraints, control increment constraints, and output constraints must be met:

$$\text{s.t.} \begin{cases} u_{\min}(t+k\,|\,t) \le u(t+k\,|\,t) \le u_{\max}(t+k\,|\,t), \\ \Delta u_{\min}(t+k\,|\,t) \le \Delta u(t+k\,|\,t) \le \Delta u_{\max}(t+k\,|\,t), \\ k = 0, 1, \ldots, N_c - 1, \\ \eta_{\min}(t+k\,|\,t) - \varepsilon \le \eta(t+k\,|\,t) \le \eta_{\max}(t+k\,|\,t) + \varepsilon. \end{cases} \tag{32}$$

Solving the above optimization problem will get the input increment in the control time domain: $\Delta U_t^* = [\Delta u_t^*, \Delta u_{t+1}^*, \ldots, \Delta u_{t+N_c-1}^*]^T$. In each step, the first element in the control increment is taken as the input of the system, and the control system executes this input until the next step. Through continuous feedback optimization, a new control increment sequence is obtained for each cycle, and the cycle ends until the system completes the optimization of the entire control process.

4.1.2. Parameter Optimization. Controller parameters are usually adjusted by engineering experience, which takes a long time. Genetic algorithm is a heuristic swarm intelligence optimization algorithm, which has fast convergence speed and is not easy to fall into a local optimum. This article

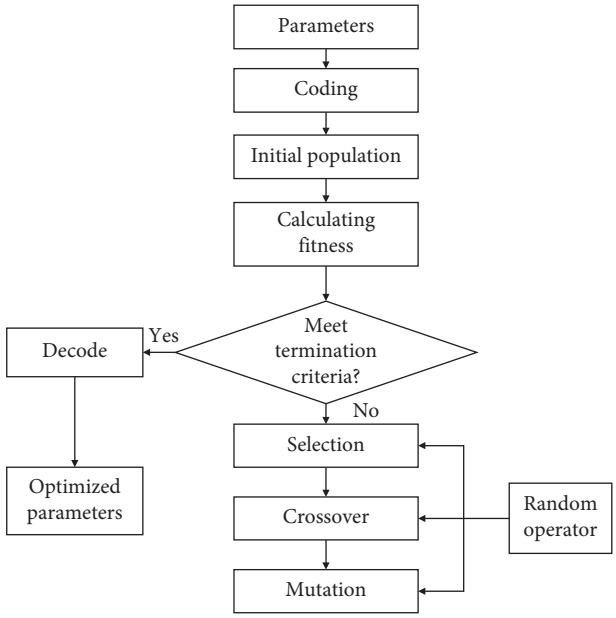

Figure 8: Flowchart of the genetic algorithm.

uses genetic algorithms to optimize the parameters in the MPC controller. The algorithm flow diagram is shown in Figure 8.

The parameters are first encoded and the initial population is generated. The parameters to be optimized include the prediction time domain, the control time domain, and the weighting matrix. Randomly generate P_N initial string structure data in the parameter solution space (i.e., one chromosome), set the maximum number of iterations k, and randomly generate P_M chromosomes as the initial population $P(0)$. The fitness function maps the quality of the solution. Considering the stability, accuracy, and speed of the system, the following fitness function is used:

$$J_{\text{opt}} = \frac{\sum_{i=0}^{N}\left(w_1|E_i| + w_2 u_i^2 + w_3|EY_i|\right)}{N}. \tag{33}$$

Among them, w_1, w_2, w_3 is the weight coefficient; $E_i = \sqrt{\left(\sum_{j=1}^{N_p}\left(Y(i+j) - Y_{\text{ref}}(i+j)\right)^2/N_p\right)}$ represents the tracking error at each step; u_i is the control input, that is, the MPC controller output; each step of the system overshoots $EY_i = Y(i) - Y(i-1)$, and when the overshoot exceeds a certain threshold, this index is used as an index in the fitness function; when it is not exceeded, $w_3 = 0$. The smaller the fitness value is, the better the solution is.

The genetic algorithm calls the controller model a subfunction. The parameters of the genetic algorithm are set as follows: population size $P_M = 20$, number of iterations $k = 50$, and weight $w_1 = 0.9, w_2 = 0.1, w_1 = \begin{cases} 0, & EY_i < EY_{\text{threshold}} \\ 10, & EY_i \geq EY_{\text{threshold}} \end{cases}$.

4.2. Self-Adaptive Fuzzy PID Dynamics Controller. The tractor-aircraft system has a complicated working environment on the deck and is prone to unstable driving under external interference. Therefore, it is necessary to regulate the stability of the system. The yaw rate and the centroid yaw angle can reflect the yaw stability of the tractor, so they are selected as the control variables. In this process, by adding a yaw moment to the tractor, the actual state and ideal state deviation of the centroid yaw angle and yaw rate during the tractor's driving process are controlled as targets, so that the system is stable within a reasonable range.

Design a fuzzy PID controller with the control variable error and error change rate as input signals. The PID parameters are adjusted online by the fuzzy controller, so that the center of mass sideslip angle and yaw rate tend to ideal values. The control structure diagram of the control system is shown in Figure 9, where ω_{r_1} is yaw rate of ideal model and β_{r_tractor} is the centroid yaw angle of ideal model.

The ideal transfer function and ideal state space equation of the system are

$$X_r(s) = \begin{bmatrix} \beta_{r\_\text{tractor}}(s) \\ \omega_{r\_1}(s) \end{bmatrix} = \begin{bmatrix} \dfrac{k_\beta}{1 + t_\omega s} \\ \dfrac{k_\omega}{1 + t_\omega s} \end{bmatrix} \psi(s), \tag{34}$$

$$\dot{X}_r = A_r X_r + C_r \psi, \tag{35}$$

where

$$A_r = \begin{pmatrix} -\dfrac{1}{t_\beta} & 0 \\ 0 & -\dfrac{1}{t_\omega} \end{pmatrix},$$

$$C_r = \begin{bmatrix} b_r + \dfrac{k_\beta}{t_\beta} \\ \dfrac{k_\omega}{t_\omega} \end{bmatrix},$$

$$k_\beta = \frac{c_1 a_{22} - a_{12} c_2 + a_{12} h_2 z_1}{a_{11} a_{22} - a_{12} a_{21}}, \tag{36}$$

$$z_1 = \frac{a_{22} c_1 + a_{12} c_2}{a_{12} h_2},$$

$$t_\beta = \frac{1}{(z h_1 - c)} k_\beta,$$

$$k_\omega = \frac{(a_{21} h_1 - a_{11} h_2) z - a_{21} c_1 - a_{12} c_2}{a_{11} a_{22} - a_{12} a_{21}},$$

$$t_\omega = \frac{1}{(c_2 + z h_2)} k_\omega.$$

Because the differential term $\dot{\psi}$ is added to the dynamics model (18), there is a constant in C_r of the state equation, which is the structural parameter b_r of the tractor system.

According to the ideal state space equation, the ideal sideslip angle and ideal yaw rate X_r can be estimated. The

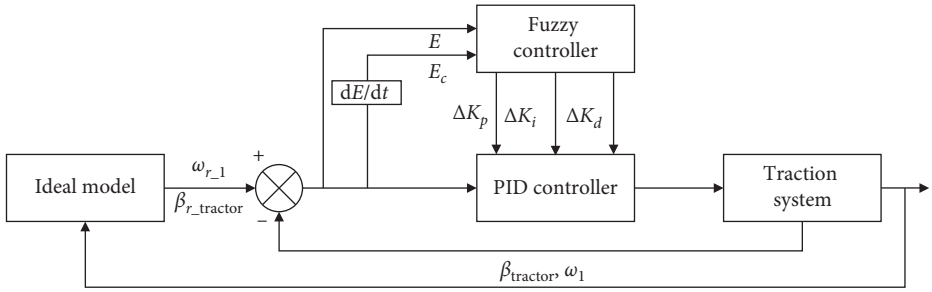

Figure 9: Adaptive fuzzy PID controller structure.

deviation of the actual control variable from the ideal control variable is

$$e(k) = X'(k) - X_r(k). \tag{37}$$

The function of deviation evaluation index is

$$E(k) = e(k)^T Q e(k). \tag{38}$$

Let $Q = [1\,0; 0\,1]$. The additional yaw moment is

$$M_f(k) = \left(K_p + \Delta K_p\right) \cdot E(k) + \left(K_i + \Delta K_i\right) \cdot \sum_{i=0}^{k} E(k) + \left(K_d + \Delta K_d\right) \cdot [E(k) - E(k-1)], \tag{39}$$

where K_p, K_i, and K_d are PID control parameters and $\Delta K_p, \Delta K_i$, and ΔK_d are fuzzy controller output parameters.

The error E and the error variety rate E_c are defined as the discourse domain on the fuzzy set U_1, both of which are $\{-1, -0.8, \ldots, 0.8, 1\}$, and the output variable domain U_2 is $\{-3, -2, -1, 0, 1, 2, 3\}$. The membership function is shown in Figures 10 and 11. The input and output fuzzy subsets are defined as {NB, NM, NS, ZE, PS, PM, PB}. The membership functions are all triangles. This sharper membership function has higher resolution and sensitivity.

To ensure the real-time control, the fuzzy control rule table is obtained by offline calculation. With reference to the general experience of fuzzy adaptive control strategies, the fuzzy control rules are given in Table 1.

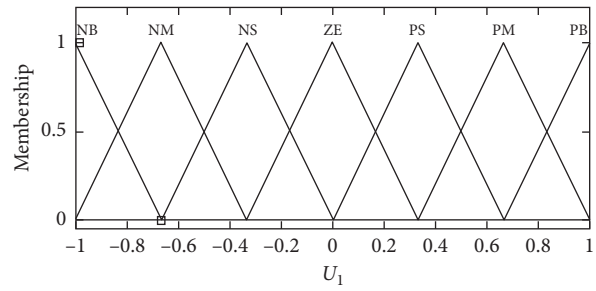

Figure 10: Membership function of input universe.

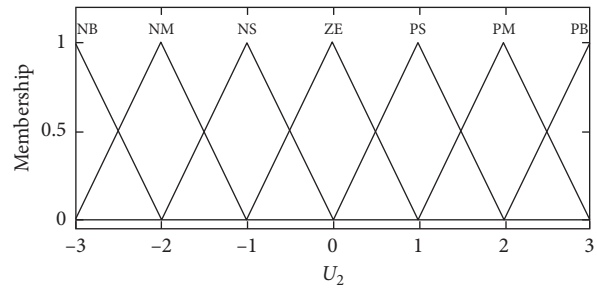

Figure 11: Membership function of output universe.

Table 1: Fuzzy control rules.

E_c \ E	NB	NM	NS	ZE	PS	PM	PB
NB	PB	PB	PM	PM	PS	PS	ZE
NM	PB	PB	PM	PS	PS	ZE	ZE
NS	PB	PM	PM	PS	ZE	NS	NS
ZE	PM	PM	PA	ZE	NS	NS	NM
PS	PM	PS	ZE	NS	NS	NM	NM
PM	PS	ZE	NS	NS	NM	NM	NB
PB	ZE	NS	NS	NM	NM	NB	NB

5. Simulation and Analysis

In order to verify the accuracy and stability of the controller, the classic trajectory and deck travel task trajectory in the tracking problem were simulated respectively, and their tracking effects were compared.

5.1. Classical Trajectories

5.1.1. Line Trajectory with Initial Deviation. According to the movement of the carrier-based aircraft on the deck, set the connection parameters $L_1 = 1, L_2 = 0.2$, traction speed constraints $|v| \le 2\text{m/s}$, acceleration constraints $|a| \le 2\text{m/s}^2$, and front wheel steering angle incremental constraints $|\Delta\delta| \le 1$. Assuming the initial states $[\theta_1, x_2, y_2, \theta_2]^T = [0, 0, 0, 0]^T$, the above controller is employed to control the traction system to track the expected straight line. The simulation results are as shown in Figure 12.

It can be seen that the system is adjusted by the controller in about 2 s, which completely suppresses the initial error and achieves accurate tracking of the linear trajectory.

In order to display the effect of different initial deviations on the system, different initial deviation combinations shown in Table 2 were used for simulation. The results obtained are as follows.

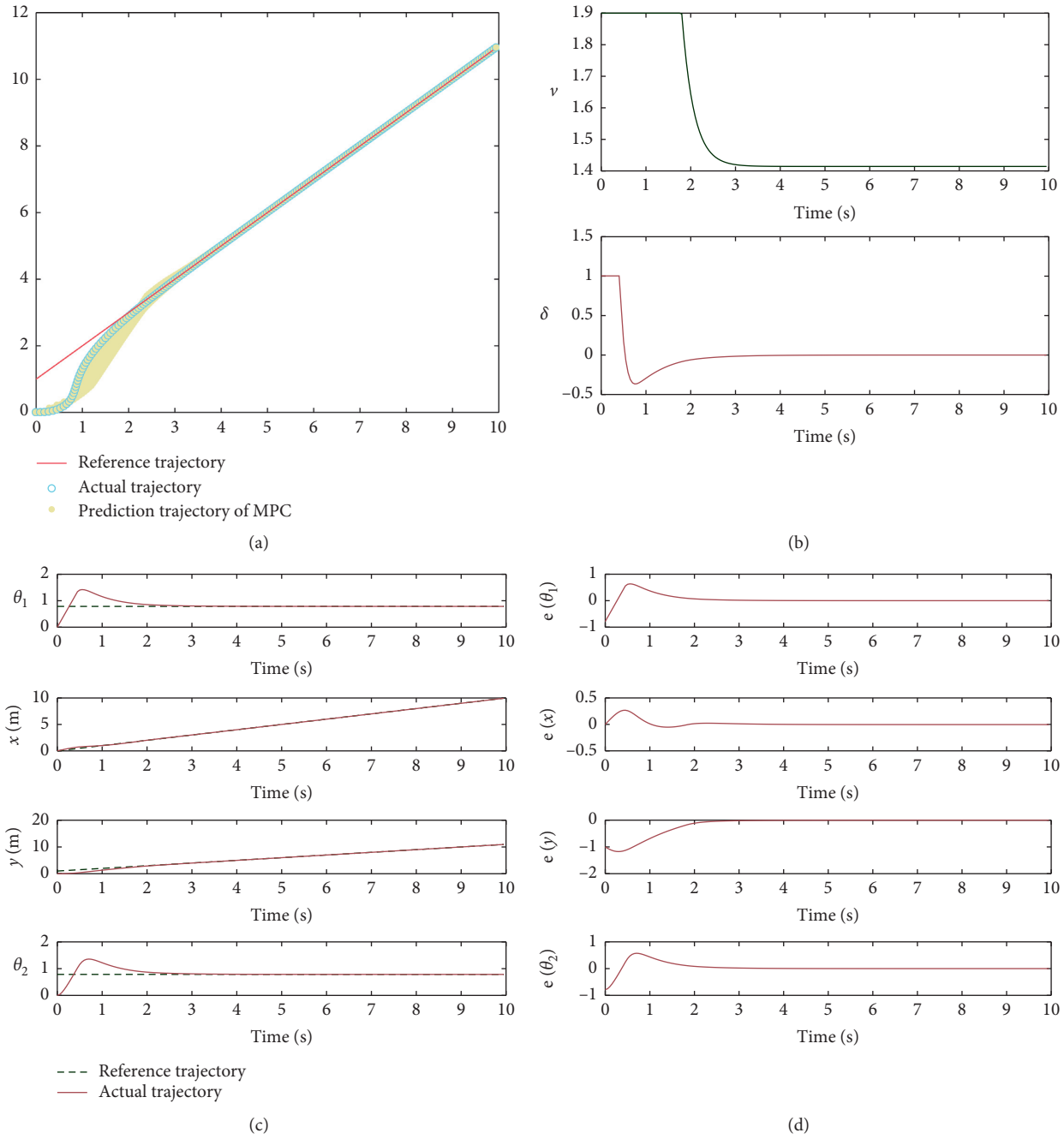

Figure 12: Simulation results of line trajectory with initial deviation. (a) Linear trajectory tracking result. (b) Changes of control variables. (c) Changes of state variables. (d) Tracking errors of state variables.

Table 2: The parameters of initial deviation.

	$\Delta\theta_1$	Δx	Δy	$\Delta\theta_2$
1	0.1	0.5	−2.0	0.1
2	0.1	−0.5	3.0	0.1
3	0.1	−0.5	−4.0	0.1
4	1	0	−1.0	1

Figures 13(a)–13(d) show the errors of the tractor's orientation angle, aircraft's abscissa, aircraft's ordinate, and aircraft's yaw angle under different initial errors, respectively. Although the system has some overshoot when the initial error is too large, the suppression of the initial error is basically completed within 5 s in all four cases. In

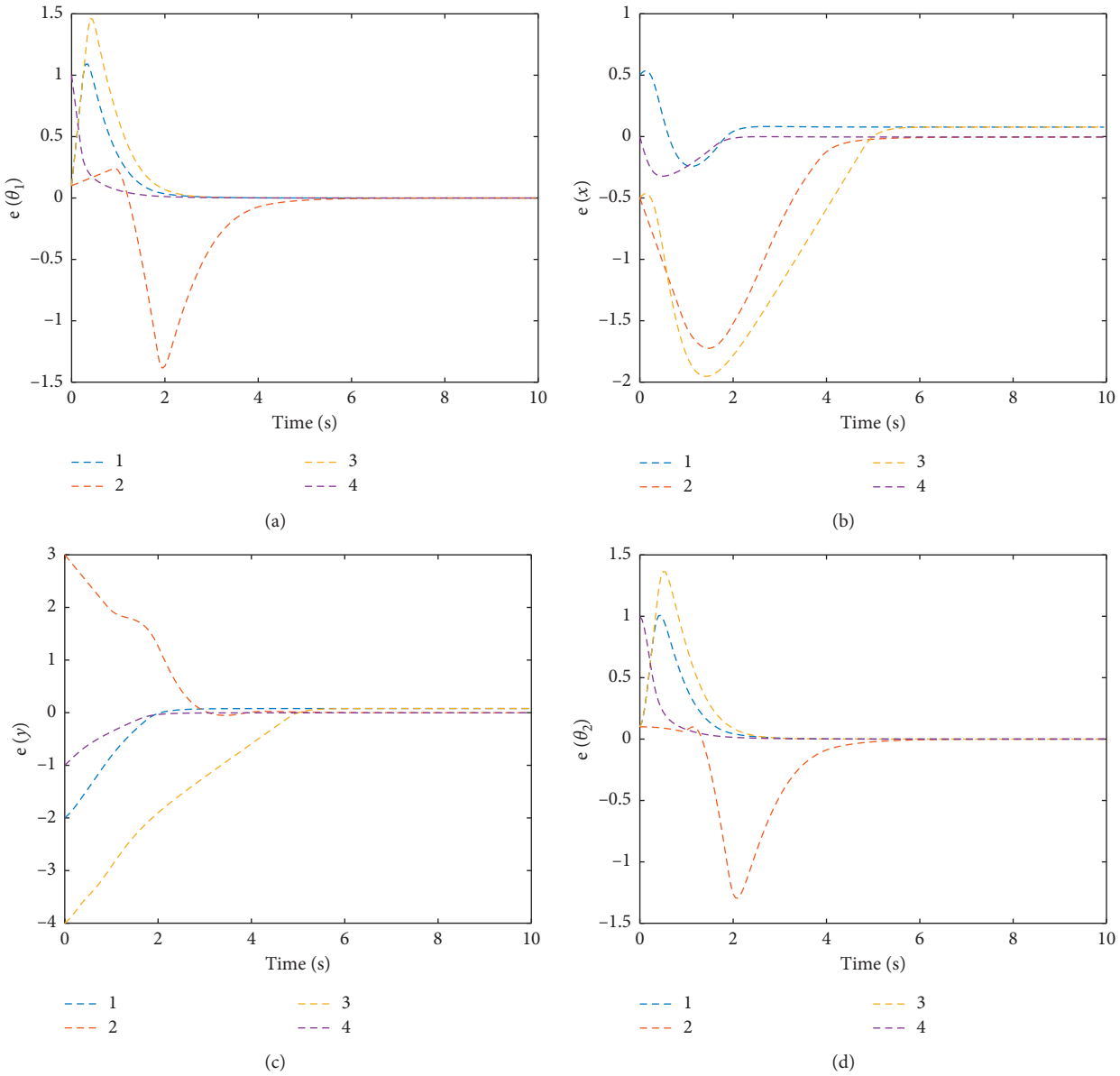

Figure 13: $e(\theta_1), e(x), e(y), e(\theta_2)$ for different initial deviation.

addition, the control input changes smoothly and is constantly adjusted within the bounds to achieve the optimum. The simulation shows that the control algorithm in this paper can quickly suppress the initial error of the linear trajectory without the steady-state error.

5.1.2. Sine Curve with Large Curvature

(1) MPC Results. Assume that the connection parameters $L_1 = 1, L_2 = 0.2$, traction speed constraint $|v| \leq 5\text{m/s}$, acceleration constraint $|a| \leq 2\text{m/s}^2$, and front wheel steering angle incremental constraint $|\Delta\delta| \leq 1$. Assuming the initial error is 0, the above controller is used to control the traction system to track a sine curve with a large curvature.

As can be seen from Figures 14(a)–14(d), the designed controller can always move forward and the tracking error in the horizontal and vertical directions does not exceed 1. The input variable is continuously adjusted within the constraint range. Due to the large curvature of the curve, the steering angle of the front wheel needs to be continuously adjusted. Overshoot occurs only when the steering angle needs to be adjusted significantly, and good performance of the system is shown in other times.

(2) Track Tracking with Initial Deviation. Similarly, in order to show the influence of the initial deviation on the sine curve's tracking, four different initial deviation parameters shown in Table 3 are mainly selected for simulation. The simulation result is shown in Figure 15.

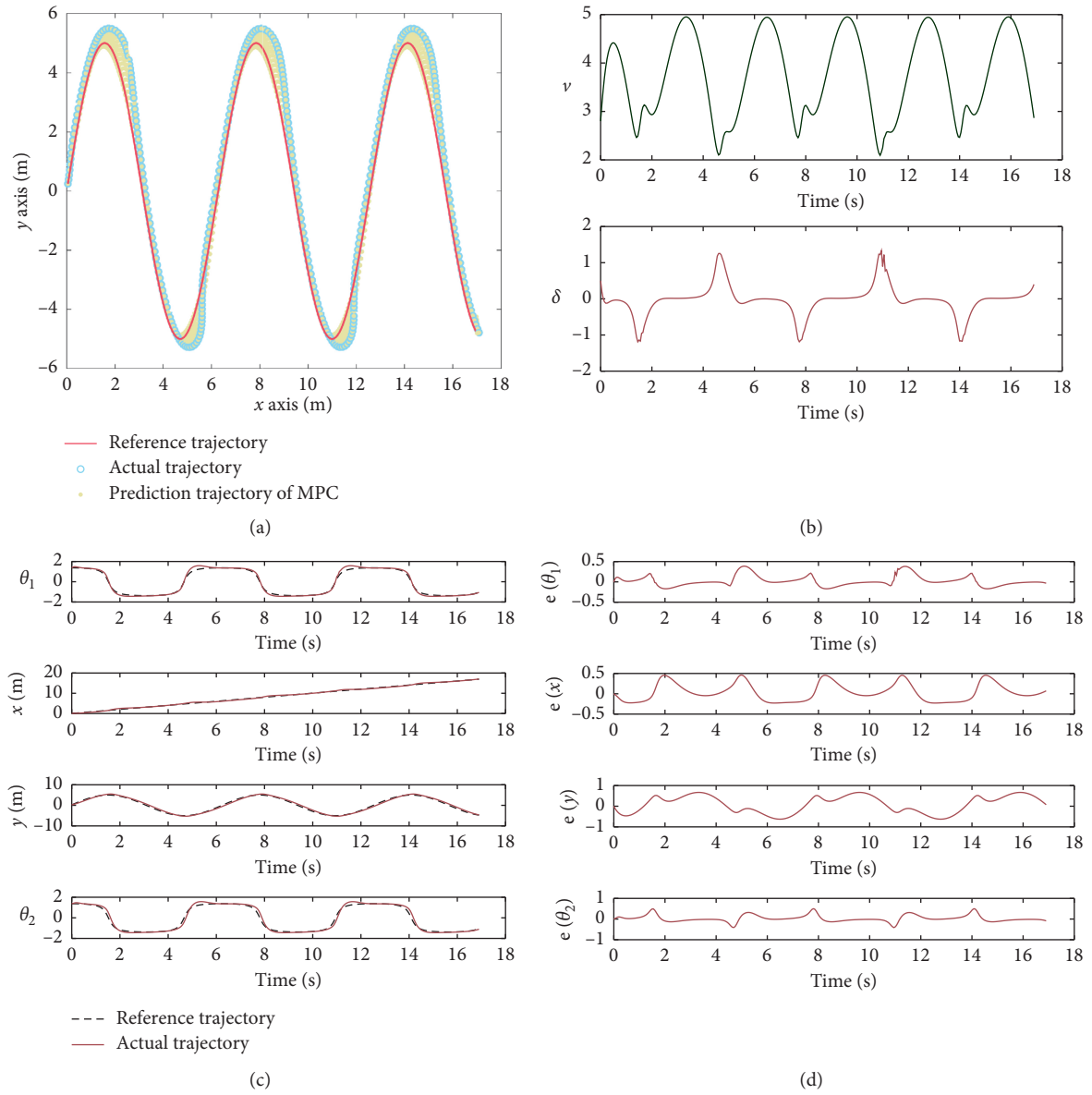

Figure 14: Simulation result of sine curve with large curvature. (a) Sine curve tracking result. (b) Changes of control variables. (c) Changes of state variables. (d) Tracking errors of state variables.

Table 3: The parameters of initial deviation.

	$\Delta\theta_1$	Δx	Δy	$\Delta\theta_2$
1	0.1	0.5	0.5	0.1
2	0.1	1.0	1.0	0.1
3	0.6	0.5	0.5	0.6
4	1	0.5	0.5	1

From Figures 15(a)–15(d), it can be seen that when the initial horizontal and vertical coordinate errors are large, the system will have some overshoot, while other cases can gradually converge to the desired trajectory within the allowable error range. In case 4, when the initial angle deviation reaches 1, it can also quickly converge to the target trajectory.

5.2. Deck Trajectories

5.2.1. Transfer Route between Flight Deck Stations

(1) Route via RRT Algorithm.* The task of carrier-based aircraft transfer on the flight deck requires it to move from the initial station to the target station and avoid collision

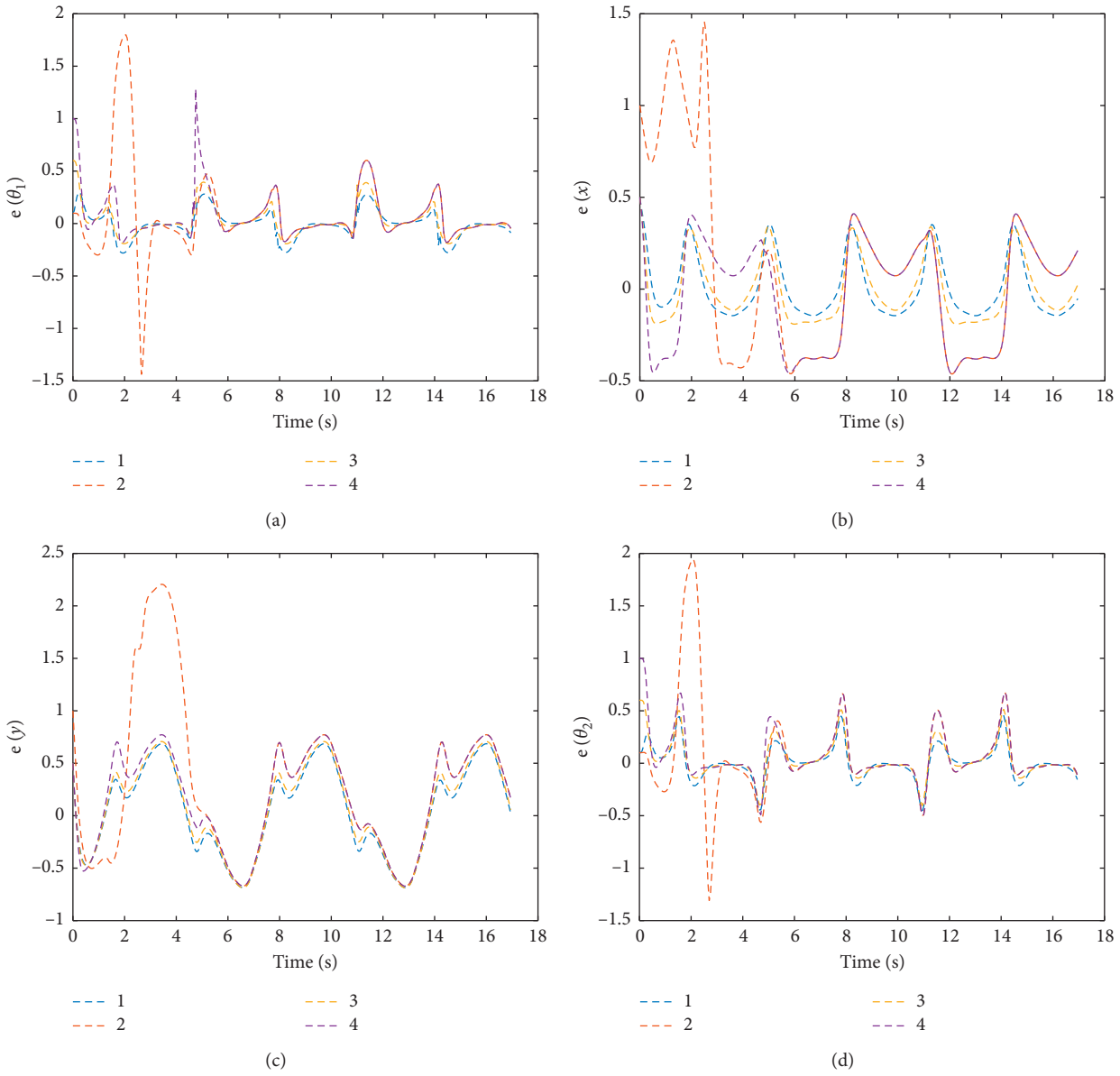

Figure 15: $e(\theta_1), e(x), e(y), e(\theta_2)$ for different initial deviation.

Table 4: Parameters for ship obstacle.

Station name	x (m)	y (m)	Direction angle (°)	Wing condition
A2	−5.500	−14.500	90	Folded wings
A3	−23.502	−13.031	90	Spread wings
A11	−76.526	32.360	342	Folded wings
Z5	−44.001	−14.500	90	Spread wings
H4	−30.328	22.999	0	Folded wings
A12	−97.526	29.861	340	Folded wings

Table 5: Parameters of traction system.

Parameter	Value
l_1 (m)	5
l_2 (m)	10
Turning radius of aircraft (m)	10
Weight of aircraft (t)	20
Wight of tractor (t)	5
Safe distance (m)	3
Initial position (m)	(12.5, −30.5)
Target position (m)	(−129.828, 7.0)

with all carrier-based aircraft parked on the deck, and a certain safety distance is required. The following figure shows an example where six carrier-based aircraft are parked on the surface of the ship. The specific parameters are shown in the Table 4 and the parameters of traction system are shown in Table 5.

The optimal Reed-Shepp path between two stations on the deck is calculated by the algorithm in Section 3.2, which meets the end position and direction requirements and can effectively avoid all obstacles. The aircraft first makes a left turn motion, and the direction angle gradually becomes larger. After the left turn is completed, it enters a linear motion. After

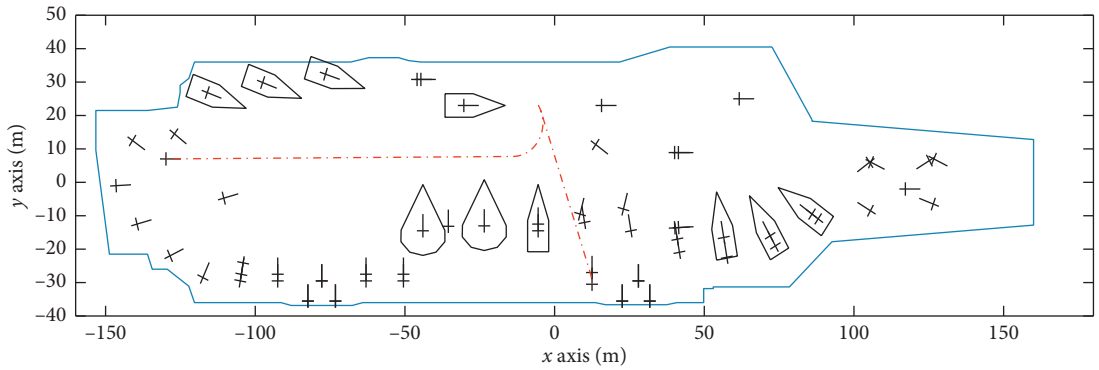

Figure 16: Path generation between stations with collision avoidance on deck.

the linear motion ends, it needs to return to the target station by reversing. The path is shown in Figure 16.

(2) Experimental Results. In order to verify the tracking effect of the controller on the deck, the above-mentioned trajectory was simulated without initial errors and the parameter optimization algorithm. Simultaneously, stability controller proposed in Chapter 3 was applied to the system.

The genetic algorithm's parameters are set as follows: population size $n = 20$, maximum iteration number $max\_gen = 50$, cross probability $p_{\text{cross}} = 0.7$, and mutation probability $p_{\text{mutation}} = 0.01$; the fitness curve and trajectory tracking results are shown in Figures 17 and 18, and the optimized parameters of the controller are shown in Table 6.

As can be seen from the above Figure 19, the algorithm can better track the expected trajectory when the system is backing up. At the beginning, due to the large change in direction angle, the steering angle of the front wheel changes rapidly, and it can be quickly stabilized in the straight phase. When entering the back-up phase, the control input can be adjusted quickly. The carrier-based aircraft keeps up with the reference trajectory and immediately stabilizes. The error converges to zero. It shows that the control algorithm in this paper can track the motion trajectory of the carrier-based aircraft on the deck well. At the same time, due to the chattering phenomenon of turning vehicles, the stability of the tractor after control is better than the data before dynamics control. This stability is mainly reflected in the fact that the yaw angular velocity and centroid skew angle after the yaw moment control can meet the requirements of vehicle handling stability better than before.

For the purpose of studying whether the controller can achieve good robustness in the presence of errors, different initial deviation combinations are used for the above simulation experiments. The main initial deviations are as follows.

The error change curves in the four cases are shown in Figure 20. It can be seen that, in the four cases, the final system can gradually converge to a stable state. The direction angle deviation and the system overshoot of case 4 are large, but it can accurately track to the predetermined position after about 10 s. For cases 1–3, the corresponding error changes are relatively gentle, indicating that, for this complex trajectory, the algorithm proposed in this paper can effectively suppress the initial error.

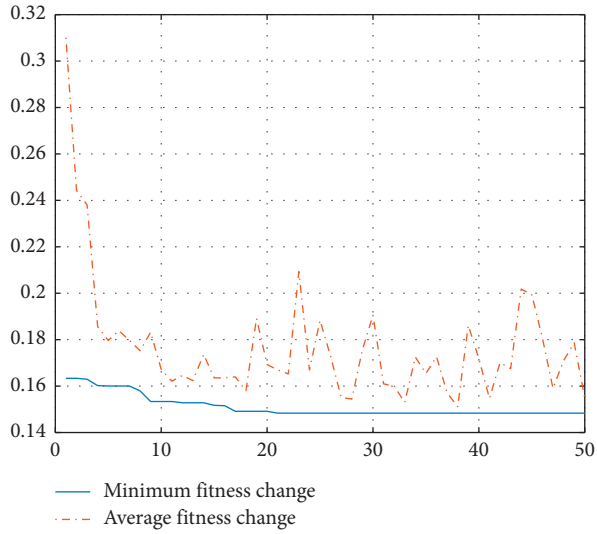

Figure 17: Fitness curve of GA.

5.2.2. Route between Recycling Station and Waiting Station

(1) Route via RRT Algorithm*. After landing on the flight deck, the carrier-based aircraft will dock at the recycling station. If the carrier-based aircraft is to prepare for the next wave of take-off, it needs to be towed to a waiting position for subsequent support operations. Assume the following situation of obstacles; the RTT* algorithm is applied to generate the traction route from the recycling station to the waiting station as shown in Figure 21.

(2) Experimental Results. Without the initial error, the control algorithm proposed in Section 3 is used to track the above trajectory, and the tracking results are shown in Figures 22 and 23.

It can be seen from the tracking error graph that the algorithm can perform stable tracking in the straight phase, but for the instantaneous reversing path or the path with a rapidly changing direction angle, the algorithm needs an adjustment time. During 138~148 s, the tractor drags the carrier-based aircraft to make a turning movement. Since the steering angle of the tractor needs to be continuously changed during this process, the system control is more

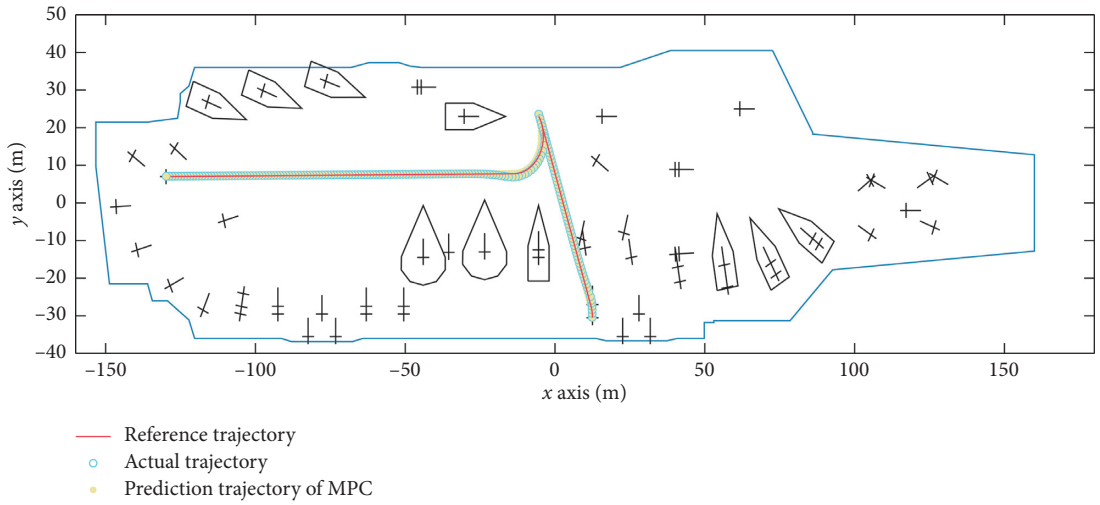

Figure 18: Trajectory tracking results between deck stations.

unstable and more sensitive to errors. The overall overshoot is within the range of [−1, 1], which is an acceptable error range for carrier-based aircraft movement. In Figures 23(d) and 23(e), after adjusting the additional torque, the overshoot of the yaw angular velocity and the center of mass side deviation angle are smaller, the adjustment time is shorter, and the system has better stability.

Similarly, simulation experiments with different initial deviation were performed on the recycling station route, and the initial deviation parameters in Table 7 were used. Figures 24(a)–24(d) are the error change curves in the four cases, and it can be seen that the four cases are all effective in suppressing the initial error. Among them, case 4 caused greater fluctuations due to the change in direction angle, but all achieved good suppression in about 20 s. This shows that the algorithm used in this paper can effectively track the complex path between the recycling station and the waiting station and meets various constraints of the system.

5.3. Controller Comparison. In order to prove the superiority of the algorithm in this paper, especially for the tracking of complex trajectories, we performed comparative simulations on the straight lines with initial deviations, the sine curves, and the trajectories between deck stations. The classical backstepping control [17] and LQR algorithm [32] are compared with the algorithm in this paper.

Figures 25–27 show the tracking trajectory and the relationship between the abscissa, ordinate, and angle error of the aircraft-tractor system over time under three algorithms. It can be analyzed from three different trajectories:

(1) For tracking of linear trajectory, both backstepping control and LQR algorithm can finally reach steady state, but the adjustment time is too long. Throughout the tracking process, the algorithm in this paper shows strong superiority, and the effect on suppressing the initial error is obviously greater than the other two algorithms.

(2) For tracking of sine curve, the errors of three algorithms have amplifying tendency at sharp turns, and they gradually stabilize on gentle road sections. Backstepping control regulates the direction angle in real time through the feedback of steering angle to minimize the error. However, it can be seen that the speed control is unsatisfactory, which results in a large lateral tracking error compared with MPC algorithm. From the graph, we can see that the LQR algorithm has obvious fluctuation, and the maximum error is more than twice that of the algorithm in this paper. The algorithm in this paper also has an advantage in tracking the sine curve.

(3) For the traction path of the towbarless tractor system on deck, LQR algorithm does not track well. The reason is that when the system changes from forward driving to reverse parking, the speed direction changes. The algorithm cannot converge to a stable state finally due to the changes during reversing, and the tracking error is larger than the algorithm proposed in this paper. As for backstepping control, the controller is not sensitive and stable to the speed's adjustment, which results in a very large overshoot.

Table 6: Controller parameters after optimization.

Parameter	Value
Sampling time: T	1
N_p	50
N_c	6
Q	[0.01 0 0 0; 0 1 0 0; 0 0 1 0; 0 0 0 1]
v_r	1.0032
δ_r	0.0032

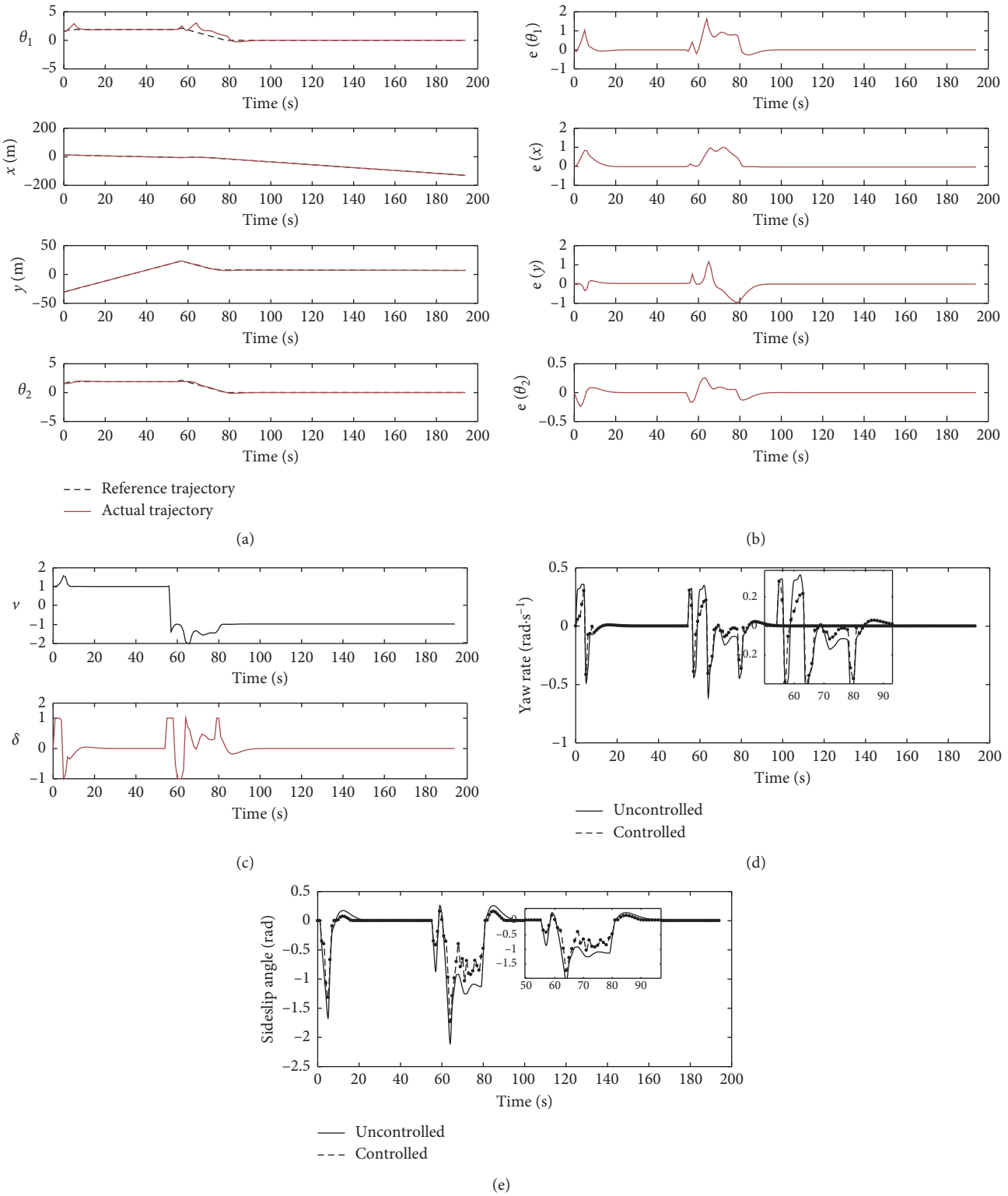

Figure 19: Tracking simulation results of transfer paths between deck stations. (a) Changes of state variables. (b) Tracking errors of state variables. (c) Changes of control variables. (d) Changes of yaw angular velocity. (e) Changes of centroid skew angle.

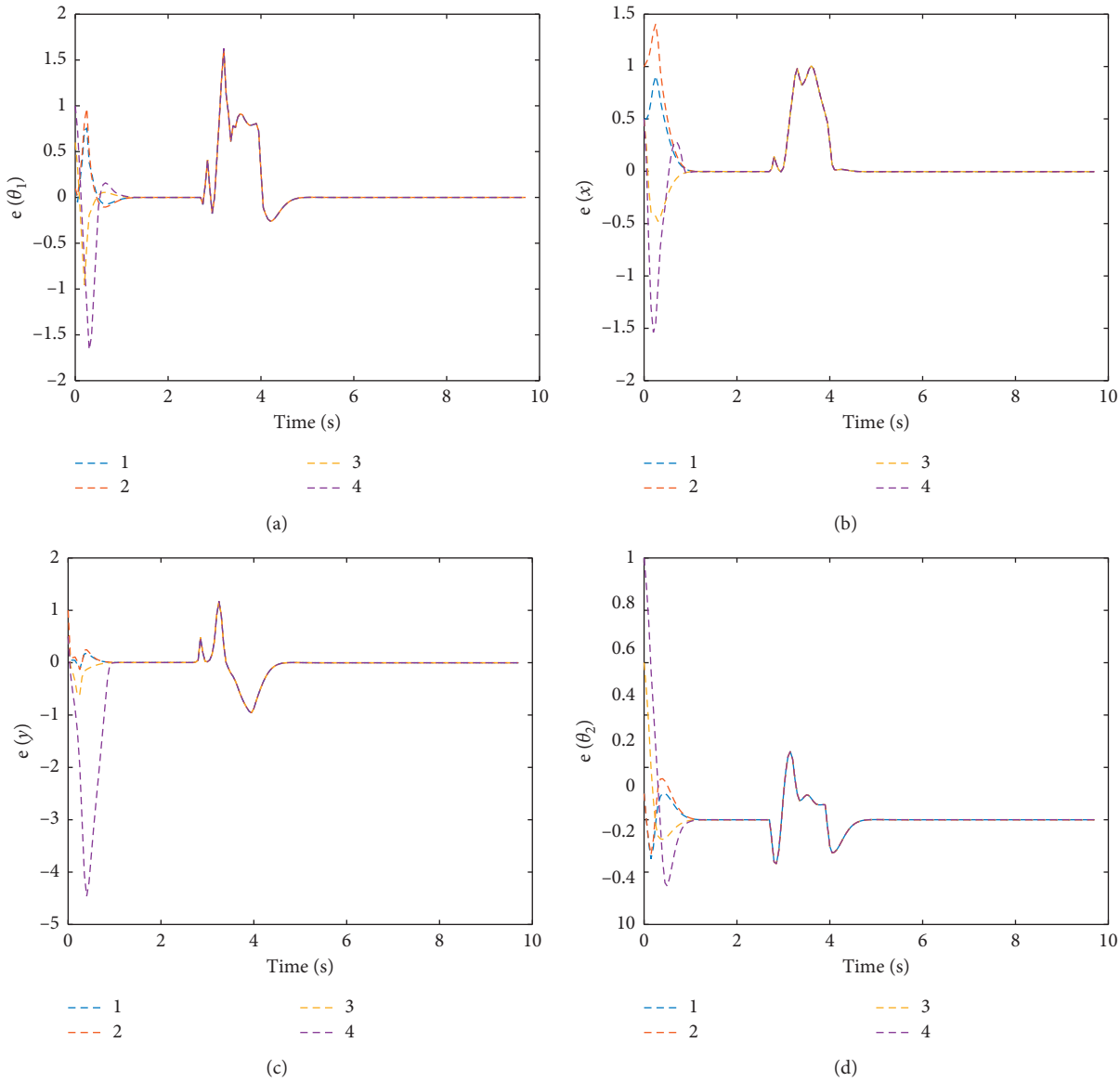

Figure 20: $e(\theta_1), e(x), e(y), e(\theta_2)$ for different initial deviation.

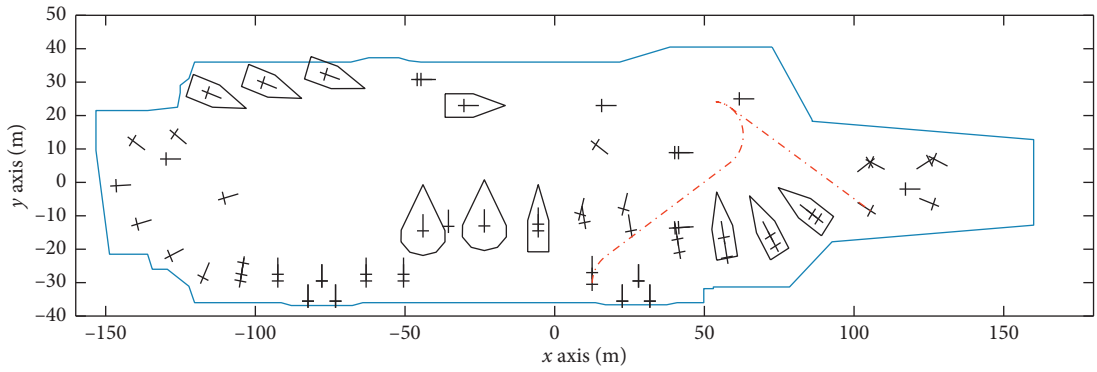

Figure 21: Path generation between recycling station and deck station.

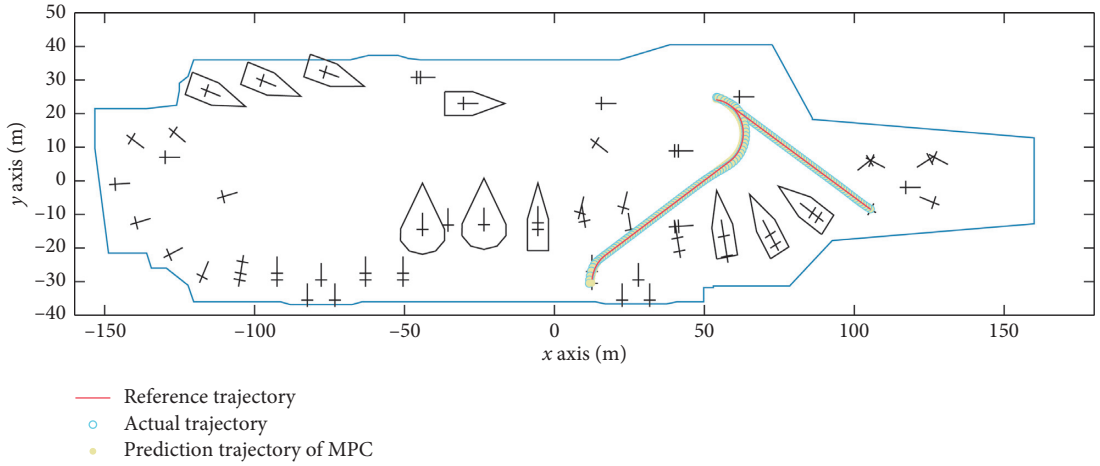

Figure 22: Trajectory tracking results between recycling station and waiting station.

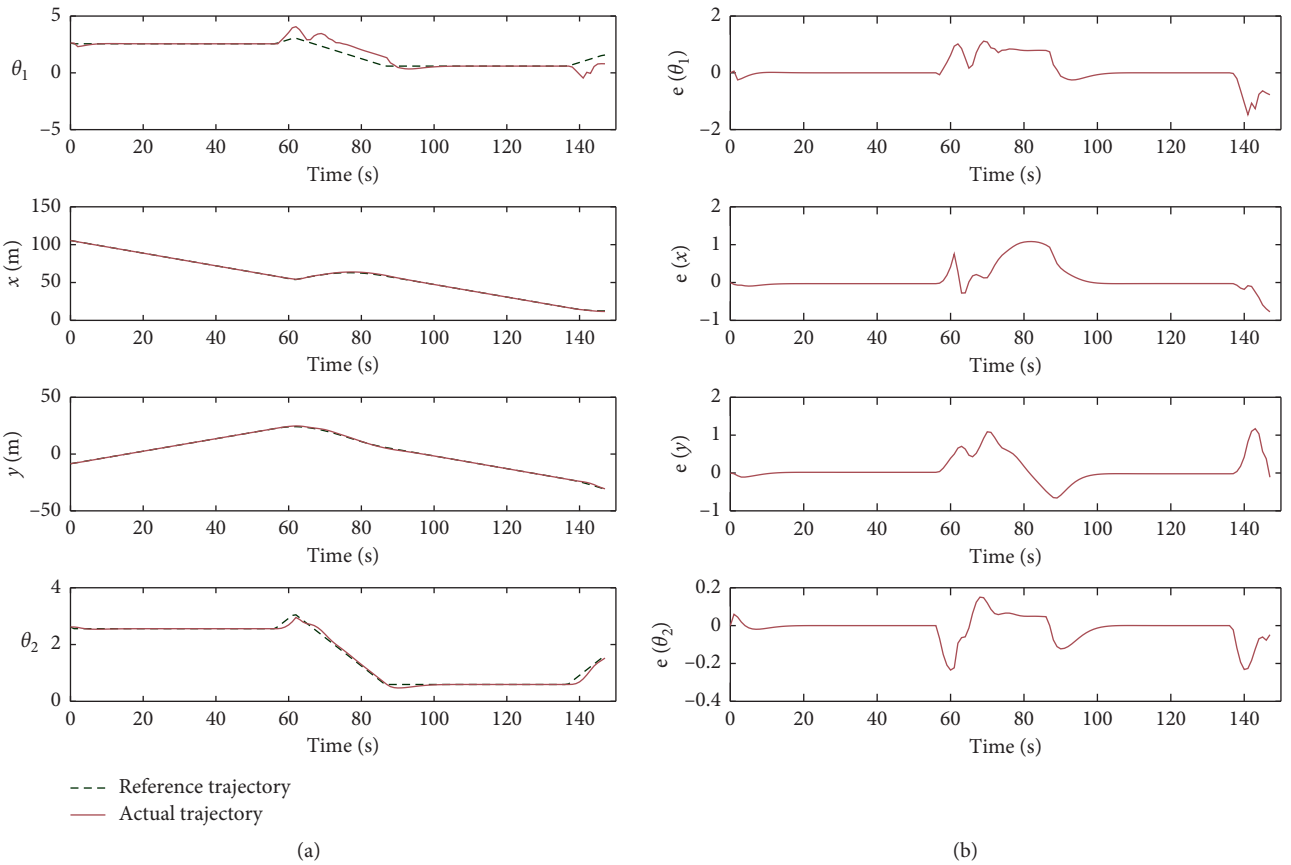

Figure 23: Continued.

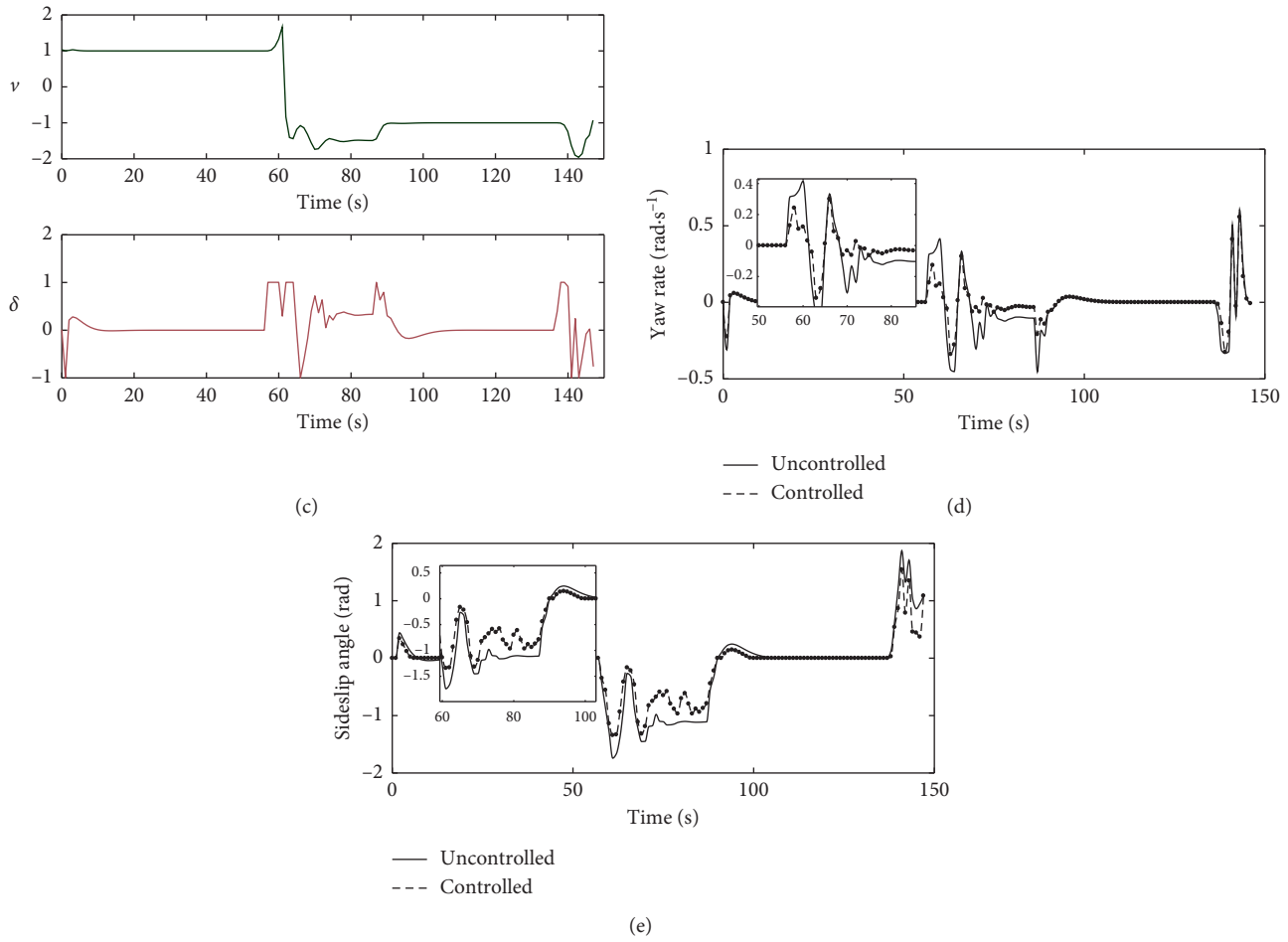

Figure 23: Tracking simulation results of transfer paths between recycling station and waiting station. (a) Changes of state variables. (b) Tracking errors of state variables. (c) Changes of control variables. (d) Changes of yaw angular velocity. (e) Changes of centroid skew angle.

Table 7: The parameters of initial deviation.

	$\Delta\theta_1$	Δx	Δy	$\Delta\theta_2$
1	0.1	0.5	0.5	0.1
2	0.1	1.0	1.0	0.1
3	0.6	0.5	0.5	0.6
4	1	0.5	0.5	1

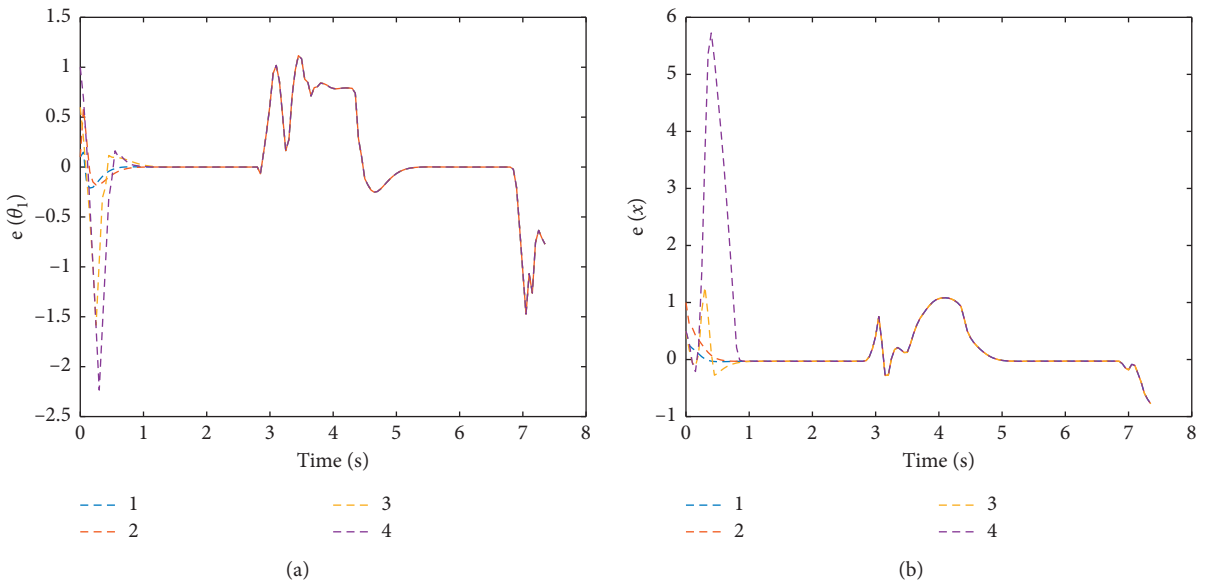

Figure 24: Continued.

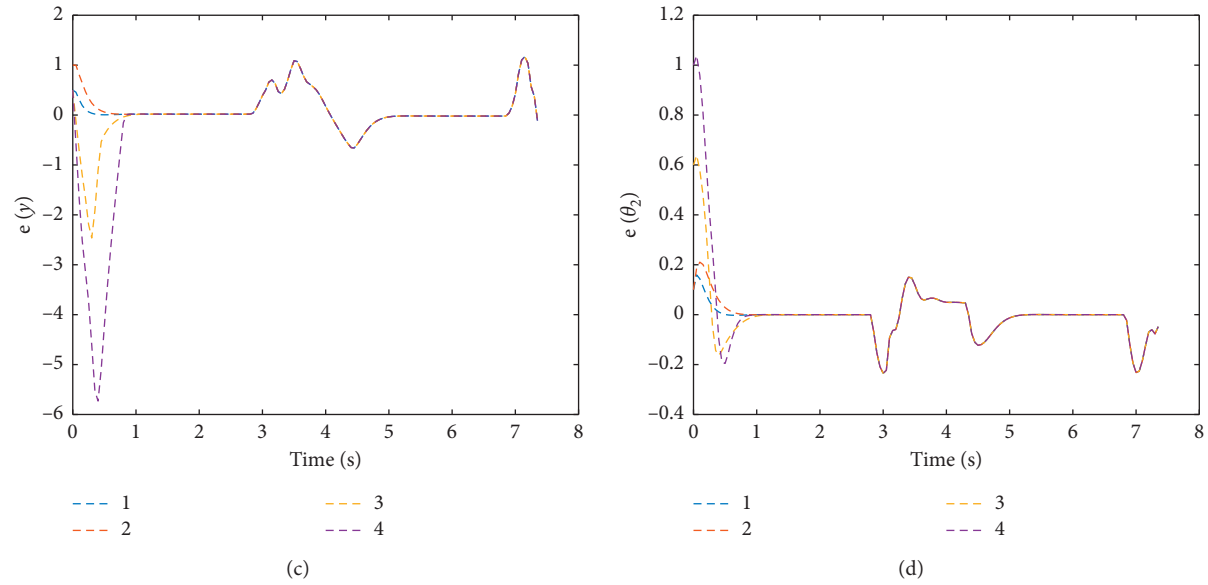

Figure 24: $e(\theta_1), e(x), e(y), e(\theta_2)$ for different initial deviation.

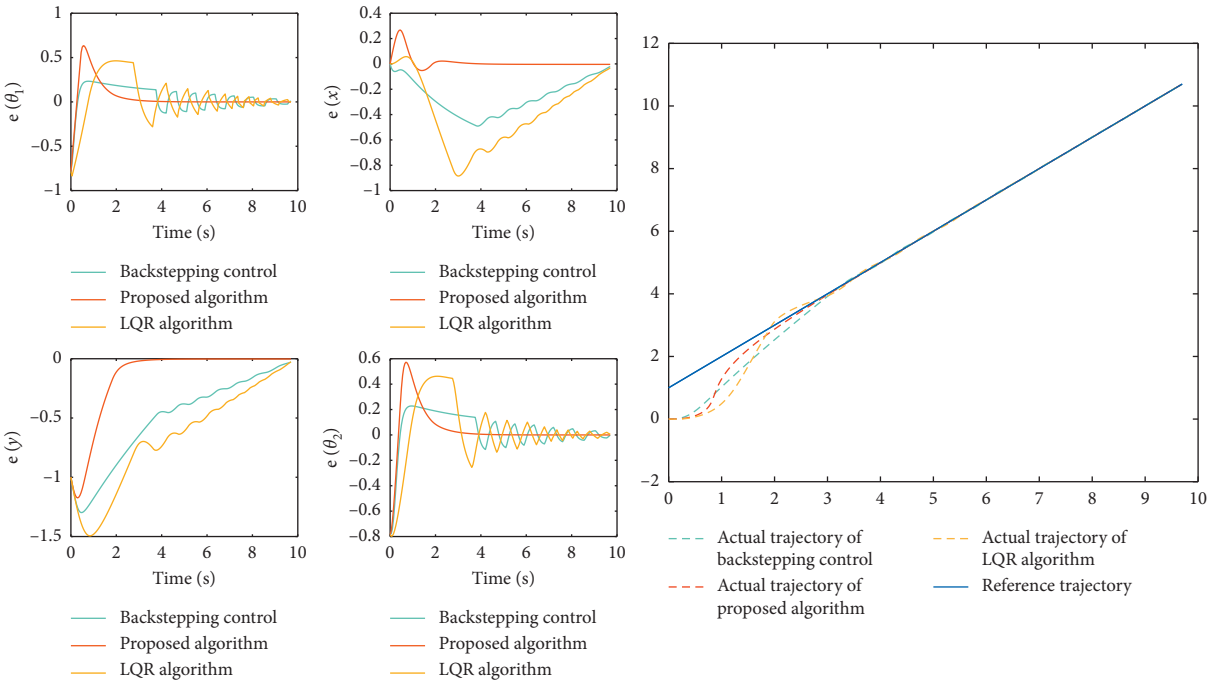

Figure 25: Line trajectories with initial deviation.

There is a certain degree of fluctuation in the second half. In contrast, the algorithm in this paper has small overshoot and fast response, which is more suitable for tracking complex trajectories on deck.

In summary, the trajectory tracking algorithm based on MPC proposed in this paper can be effectively applied to the trajectory tracking problem of towbarless traction systems.

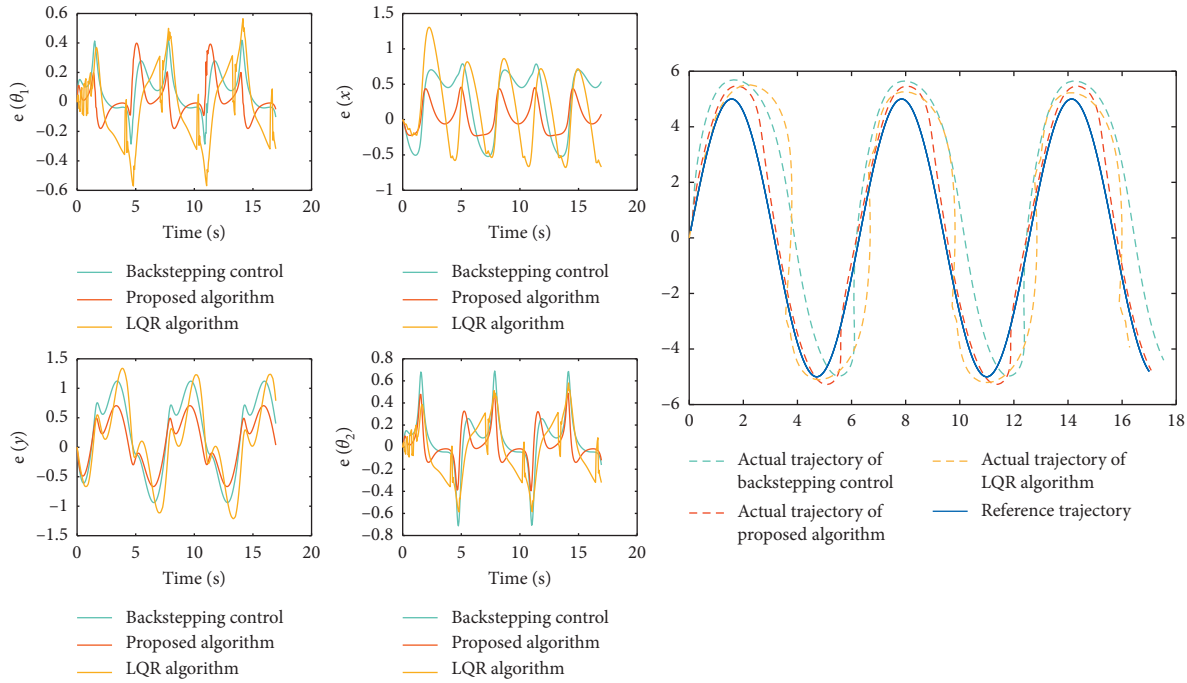

Figure 26: Sine curve with large curvature.

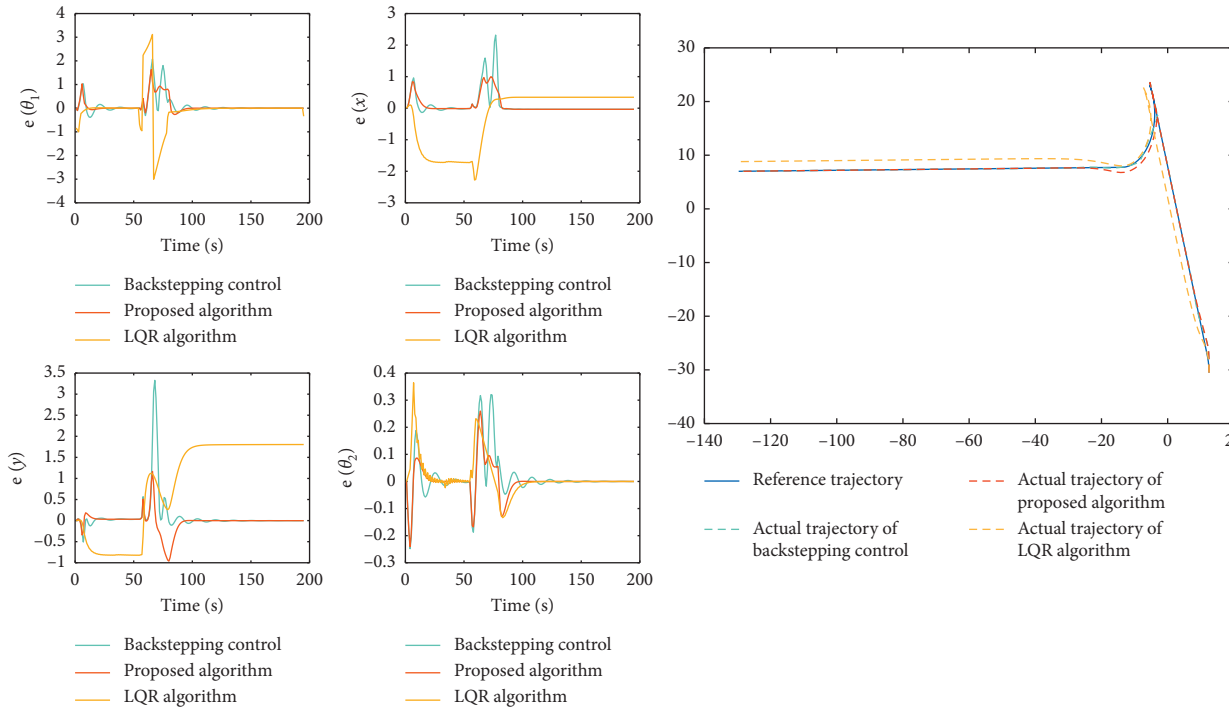

Figure 27: Deck trajectory.

6. Conclusion

In this paper, considering the nonintact constraints and various conditions, we propose a solution to the problem of tracking complex trajectories on the deck of a towbarless tractor-aircraft system. First, the strategy is proposed to control multiple aircrafts to plan trajectory cooperatively and the method based on RRT* is used to generate optimal path with obstacle. Then we construct model predictive controller (MPC) to track the reference trajectory and fully consider the dynamic performance of the system. Moreover, self-adaptive fuzzy PID controller is applied to control the

dynamics parameter to ensure the stable operation of the plane and greatly improve the anti-interference ability of the system. By tracking straight lines, sine curves with large curvature, and two complex trajectories on the deck, the controller can make the system quickly converge to the desired trajectory, which proves the robustness and accuracy of the system. At the same time, compared with feedback control and LQR control, the tracking accuracy and speed of the algorithm in this paper are far superior to the other two control methods. It shows that the traditional method finds difficulty in solving the complex state constraints and the strict control constraints at the same time. In other words, the proposed method can achieve the promising accuracy and stability and has practical application potential. In the near future, we plan to apply the algorithm in an aircraft carrier simulation system to evaluate our method in a real environment, which will be more challenging.

Data Availability

The data used to support the findings of this study are included within the article. Because of ethical concerns, the original data cannot be made openly available.

Conflicts of Interest

The authors declare that they have no conflicts of interest.

Acknowledgments

This work was supported by the National Natural Science Foundation of China under Grant no. 61403255 and the National Defense Science Foundation Project of China under Grant no. JCKY 2017207B005.

References

[1] B. Michini and J. How, "A human-interactive course of action planner for aircraft carrier deck operations," in *Proceedings of the AIAA Information Technology*, March 2011.

[2] B. Li, T. Acarman, Y. Zhang, L. Zhang, C. Yaman, and Q. Kong, "Tractor-trailer vehicle trajectory planning in narrow environments with a progressively constrained optimal control approach," *IEEE Transactions on Intelligent Vehicles*, p. 1, 2020.

[3] X. Wang, H. Su, X. Wang, and G. Chen, "Fully distributed event-triggered semiglobal consensus of multi-agent systems with input saturation," *IEEE Transactions on Industrial Electronics*, vol. 64, no. 6, pp. 5055–5064, 2017.

[4] X. L. Wang, H. Su, M. Z. Q. Chen, X. F. Wang, and G. Chen, "Reaching non-negative edge consensus of networked dynamical systems," *IEEE Transactions on Cybernetics*, vol. 48, no. 9, pp. 2712–2722, 2018.

[5] X. L. Wang, H. Su, M. Z. Q. Chen, and X. Wang, "Observer-based robust coordinated control of multi-agent systems with input saturation," *IEEE Transactions on Neural Networks and Learning Systems*, vol. 529, no. 5, pp. 1933–1946, 2018.

[6] Y. Liu and H. Su, "Containment control of second-order multi-agent systems via intermittent sampled position data communication," *Applied Mathematics and Computation*, vol. 362, no. 362, p. 124522, 2019.

[7] X. Wang and H. Su, "Self-triggered leader-following consensus of multi-agent systems with input time delay," *Neurocomputing*, vol. 330, pp. 70–77, 2019.

[8] Y. Liu and H. Su, "Some necessary and sufficient conditions for containment of second-order multi-agent systems with sampled position data," *Neurocomputing*, vol. 378, no. 378, pp. 228–237, 2020.

[9] R. Kong, "Accurate parking planning of tractor-trailer-trailer mobile robot," in *Proceedings of the 2012 IEEE International Conference on Mechatronics and Automation*, pp. 1220–1226, IEEE, Chengdu, China, August 2012.

[10] N. T. Binh, N. A. Tung, D. P. Nam, and N. H. Quang, "An adaptive backstepping trajectory tracking control of a tractor trailer wheeled mobile robot," *International Journal of Control Automation and Systems*, vol. 17, no. 2, pp. 465–473, 2019.

[11] J. Cai, H. Jiang, L. Chen, J. Liu, Y. Cai, and J. Wang, "Implementation and development of a trajectory tracking control system for intelligent vehicle," *Journal of Intelligent & Robotic Systems*, vol. 94, no. 1, pp. 251–264, 2019.

[12] Y. Wu, L. Sun, and X. Qu, "A sequencing model for a team of aircraft landing on the carrier," *Aerospace Science and Technology*, vol. 54, pp. 72–87, 2016.

[13] D. Wu, Q. Zhang, and J. F. Reid, "Adaptive steering controller using a Kalman estimator for wheel-type agricultural tractors," *Robotica*, vol. 19, no. 5, pp. 527–533, 2001.

[14] E. Kayacan, E. Kayacan, H. Ramon, O. Kaynak, and W. Saeys, "Towards agrobots: trajectory control of an autonomous tractor using type-2 fuzzy logic controllers," *IEEE/ASME Transactions on Mechatronics*, vol. 20, no. 1, pp. 287–298, 2015.

[15] A. K. Khalaji and S. A. A. Moosavian, "Robust adaptive controller for a tractor-trailer mobile robot," *IEEE/ASME Transactions on Mechatronics*, vol. 19, no. 3, pp. 943–953, 2014.

[16] Z. Huofeng, M. Baoli, S. Lihui, and F. F. Zhang, "Path following control of tractor-trailers with off-axle hitching," *Acta Automatica Sinica*, vol. 36, no. 9, pp. 1272–1278, 2010.

[17] N. Lashkari, M. Biglarbegian, and S. X. Yang, "Backstepping tracking control design for a tractor robot pulling multiple trailers," in *Proceedings of the 2018 Annual American Control Conference (ACC)*, pp. 2715–2720, IEEE, Milwaukee, WI, USA, June 2018.

[18] R. Werner, G. Kormann, and S. Mueller, "Systematic model based path tracking control of actively steered implements in simulation and experiment," *IFAC Proceedings Volumes*, vol. 46, no. 18, pp. 85–90, 2013.

[19] Y. Bin, T. Shim, F. Nenglian, and D. Zhou, "Path tracking control for backing-up tractor-trailer system via model predictive control," in *Proceedings of the 24th Chinese Control and Decision Conference (CCDC)*, pp. 198–203, IEEE, Taiyuan, China, 2012.

[20] M. Yue, X. Hou, M. Fan, and R. Jia, "Coordinated trajectory tracking control for an underactuated tractor-trailer vehicle via MPC and SMC approaches," in *Proceedings of the 2nd International Conference on Advanced Robotics and Mechatronics (ICARM)*, pp. 82–87, IEEE, Hefei, China, August 2017.

[21] E. Kayacan, H. Ramon, and W. Saeys, "Robust trajectory tracking error model-based predictive control for unmanned ground vehicles," *IEEE/ASME Transactions on Mechatronics*, vol. 21, no. 2, pp. 806–814, 2016.

[22] J. Backman, T. Oksanen, and A. Visala, "Navigation system for agricultural machines: nonlinear model predictive path tracking," *Computers and Electronics in Agriculture*, vol. 82, no. 82, pp. 32–43, 2012.

[23] E. Kayacan, E. Kayacan, H. Ramon, and W. Saeys, "Learning in centralized nonlinear model predictive control: application to an autonomous tractor-trailer system," *IEEE Transactions on Control Systems Technology*, vol. 23, no. 1, pp. 197–205, 2015.

[24] H. Fan, S. Li, H. Ding, and J. Zhang, "Simulation analysis of vehicle trajectory tracking based on model predictive control," in *Proceedings of the 2009 IEEE 28th International Symposium on Industrial Electronics (ISIE)*, pp. 1892–1897, IEEE, Vancouver, BC, Canada, June 2019.

[25] N. Wang, H. Liu, and W. Yang, "Simulation study of the backward-motion for a aircraft towbarless tractor," in *Proceedings of the IEEE Conference Anthology*, pp. 1–5, IEEE, China, January 2013.

[26] M. Karkee and B. L. Steward, "Study of the open and closed loop characteristics of a tractor and a single axle towed implement system," *Journal of Terramechanics*, vol. 47, no. 6, pp. 379–393, 2010.

[27] W. Jianchun and L. Wang, "Transient and steady responses of articulated vehicle to disturbance moment(I)," *Mining and Processing Equipment*, vol. 9, no. 36, pp. 26–29, 2008.

[28] F. You, R. Zhang, G. Lie, H. Wang, H. Wen, and J. Xu, "Trajectory planning and tracking control for autonomous lane change maneuver based on the cooperative vehicle infrastructure system," *Expert Systems with Applications*, vol. 42, no. 14, pp. 5932–5946, 2015.

[29] J. M. Kim, K. I. Lim, and J. H. Kim, "Auto parking path planning system using modified Reeds-Shepp curve algorithm," in *Proceedings of the 2014 11th International Conference on Ubiquitous Robots and Ambient Intelligence (URAI)*, pp. 311–315, IEEE, Kuala Lumpur, Malaysia, November 2014.

[30] L. Han, Q. H. Do, and S. Mita, "Unified path planner for parking an autonomous vehicle based on RRT," in *Proceedings of the 2011 IEEE International Conference on Robotics and Automation*, pp. 5622–5627, IEEE, Shanghai, China, May 2011.

[31] J. Yuan, F. Sun, and Y. Huang, "Trajectory generation and tracking control for double-steering tractor-trailer mobile robots with on-axle hitching," *IEEE Transactions on Industrial Electronics*, vol. 62, no. 12, pp. 7665–7677, 2015.

[32] B. Paden, M. Cap, S. Z. Yong, D. Yershov, and E. Frazzoli, "A survey of motion planning and control techniques for self-driving urban vehicles," *IEEE Transactions on Intelligent Vehicles*, vol. 1, no. 1, pp. 33–55, 2016.